NANOPARTICLE CLEARANCE IS GOVERNED BY TH1/TH2 IMMUNITY AND STRAIN BACKGROUND

Stephen W. Jones

A dissertation submitted to the faculty at the University of North Carolina at Chapel Hill in partial fulfillment of the requirements for the degree of Doctor of Philosophy in the department of Cell Biology in the School of Medicine.

Chapel Hill
2013

Approved by

James Bear

Keith Burridge

Richard Chenny

Ian Davis

Mohanish Deshmukh

ABSTRACT

Stephen W. Jones: Nanoparticle Clearance is Governed by Th1/Th2 Immunity and Strain
(Under the direction of James E. Bear)

Extended circulation of nanoparticles in blood is essential for most clinical applications. Nanoparticles are rapidly cleared by cells of the mononuclear phagocyte system (MPS). Approaches such as grafting polyethylene glycol onto particles (PEGylation) extend circulation times; however, these particles are still cleared and the processes involved in this clearance remain poorly understood. Here we present a novel assay using intravital microscopy for the quantification of nanoparticle clearance, allowing us to determine the effect of mouse strain and immune system function on particle clearance. We demonstrate that mouse strains which are prone to Th1 immune responses clear nanoparticles at a slower rate than Th2-prone mice. Using depletion strategies, we show that both granulocytes and macrophages participate in the enhanced clearance observed in Th2-prone mice. Macrophages isolated from Th1 strains take up fewer particles in vitro than macrophages from Th2 strains. Treating macrophages from Th1 strains with cytokines to differentiate them into M2 macrophages increases the amount of particle uptake. Conversely, treating macrophages from Th2 strains with cytokines to differentiate them into M1 macrophages decreases their particle uptake.

TABLE OF CONTENTS

LIST OF TABLES

LIST OF FIGURES

CHAPTER ONE: INTRODUCTION

Nanoparticles in medicine

Nanoparticles have been investigated for medicinal applications for over 40 years (Chakraborty et al., 2013). Nanoparticle use in medicine can be broadly grouped into two categories, particles used for therapeutic applications in which the particle serves as therapeutic vehicle, and particles used for diagnostic applications. For the majority of nanoparticle therapeutics the principle is to immobilize a therapeutic agent within the matrix of a nanoparticle and thereby alter the pharmacokinetics (PK) of the therapeutic agent. The guiding principle behind this is that therapeutic agents that are normally toxic, unstable, or insoluble can be sequestered within the particle until they can be released at an appropriate time and place. In most systems the particle utilizes a targeting agent such as an antibody or a DNA aptamer to direct the particle to a particular physiological destination (Beech et al., 2013; Fokong et al., 2012; Lammers et al., 2012; Li et al., 2013b; Shin et al., 2013). Once present in the desired location in the body the particle either degrades naturally or is triggered to degrade by altered physiological conditions such as low pH, reducing environment, or enzymatic activity. The degrading particle releases the encapsulated therapeutic agent upon degradation thereby targeting the majority of the agent to the site of

physiological interest and limiting off target effects (Morachis et al., 2012b). For diagnostic applications particles are functionalized with materials that can be detected with medical technology such as radiolabels for PET/SPECT imaging, MRI contrast agents, or fluorophores for fluorescent imaging (Feng et al., 2013; Gu et al., 2013; Wadajkar et al., 2013). Again in most circumstances diagnostic nanoparticles are conjugated with targeting agents to direct them to a site of interest in the body to aid physicians in the diagnosis and assessment of pathological conditions. Despite decades of work and thousands of papers published on the topic of nanomedicine, only two nanoformulations have been approved for clinical use in the USA. Abraxane which is a naoparticle formulation of albumin and paclitaxel, and doxil a liposomal formulation of doxorubicin (Coleman et al., 2006; Gradishar, 2006a; Krown et al., 2004). While there is still significant hope that nanoparticles will play a major future role in the clinic it has become clear that several major hurdles still must be overcome before nanotherapies will be widely efficacious. Here we will examine issues related to the response of the immune system to nanoparticles in blood.

Classes of Nanoparticles

A wide variety of materials schemes have been developed to generate nanoparticles for medical applications. Different particles with different material properties will show quite different capacities to bind drugs or therapeutic agents, utilize targeting strategies, show varying PK, and varying toxicology. Polymeric nanoparticles (Fig 1 A), are one of the most common types being researched for

medical applications. They can be made out of a very wide variety of materials with varying properties, can be easily designed to hold drugs inside the particle, can be functionalized with surface ligands of choice, and benefit from a huge amount of chemistry and materials knowledge of polymers and their properties. However it is challenging to make polymer particles smaller than 80-100nm, and they often show a wide range of sizes within one batch (Feng et al., 2013; Morachis et al., 2012a; Zhang et al., 2013). Polymeric micells (Fig 1 B) are formed by generating a polymer shell with one surface (typically the interior) being hydrophobic and the other being hydrophilic. The interior of the particle is typically filled with an oil droplet that can dissolve large amounts of hydrophobic drugs in the hydrophobic interior. The hydrophilic exterior can then be functionalized with stealthing or targeting ligands as needed. They can typically carry larger payloads of drug than polymer particles of the same size and can be made smaller, down to about 20nm. But they are often unstable i*n vivo* and it is difficult to control the release of drugs from the interior of the particle (Fokong et al., 2012; Muthiah et al., 2013; Yurgel et al., 2013). Dendrimers (Fig 1 C) are large branched single chain polymers which contain within them many binding domains for therapeutics or imaging agents within them. The dendrimer is quite small for a nanoformulation often being less than 20nm in size. The highly hydrophilic nature of dendrimers give them excellent PK, but it is difficult to load large amounts of drug on a dendrimer and difficult to effectively target them (Liu et al., 2013; Ma et al., 2013; Ravina et al., 2010; Singha et al., 2011). Liposomes (Fig 1 D) are the most studied nanoformulation for medical applications and the

first nanodrug to get full approval in US for use (Doxil) (Biganzoli et al., 2007; Coleman et al., 2006). They are created by making a lipid bilayer typically ~100nm in size that contain a water droplet on the inside that can be loaded with hydrophilic therapeutics. The outer surface of the liposome can then be functionalized with targeting agents or stealthing ligands. Liposomes are easy to make and very biologically compatible with low toxicology and good PK, but like polymeric micelles they are unstable and difficult to control drug release from (Chattopadhyay, 2013; Jolck et al., 2010; Naik et al., 2013; Qian et al., 2012). In recent years some labs have started referring to viruses as nanoparticles (Fig 1 E), which is a technically correct definition. This has caused virus mediated genetic therapies to become incorporated into nanomedicine. In addition some effort has been made to formulate viral particles that contain a drug in the interior instead of genetic material. Viruses have the advantages of excellent natural targeting, cell penetrating, and controlled delivery of cargoes. However. viruses often illicit an immune response which limits their efficacy *in vivo* and can be dangerous to the patient. It is also difficult to produce large amounts of virus (Lentz et al., 2012; Manjila et al., 2013; Sun et al., 2013b; Usme-Ciro et al., 2013). Finally carbon nanotubes (Fig 1 F), have shown some potential as diagnostic agents due to their unusual optical and magnetic properties that make them easy to detect *in vivo.* However it is difficult to get nanotubes to demonstrate good PK, and difficult to target them to sites of interest for diagnostics. There have also been several studies suggesting that nanotubes may not break down *in vivo* and can contribute long term to toxicological events

(Li et al., 2013a; Reynolds et al., 2013; Sun et al., 2013a; Tan et al., 2011; Yildirimer et al., 2011).

The PRINT® System for Nanoparticle Synthesis.

Recently a new technique known as particle replication in non-wetting templates (PRINT) has been developed for the generation of hydrogel nanoparticles with a high level of control over the size and shape of the particles (Rolland et al., 2005). This allows for more precise experiments comparing effects of size and shape on particle PK (Gratton et al., 2007), cell entry (Gratton et al., 2008a; Gratton et al., 2008c), targeting (Wang et al., 2010), PEG stealthing (Perry et al., 2012) and novel classes of microparticles (Merkel et al., 2011). In all cases by taking advantage of the nature of the PRINT system particles with limited diversity of size and shape can be compared much more rigorously than more heterogeneous particle populations, which allows for more detailed experiments with better controls.

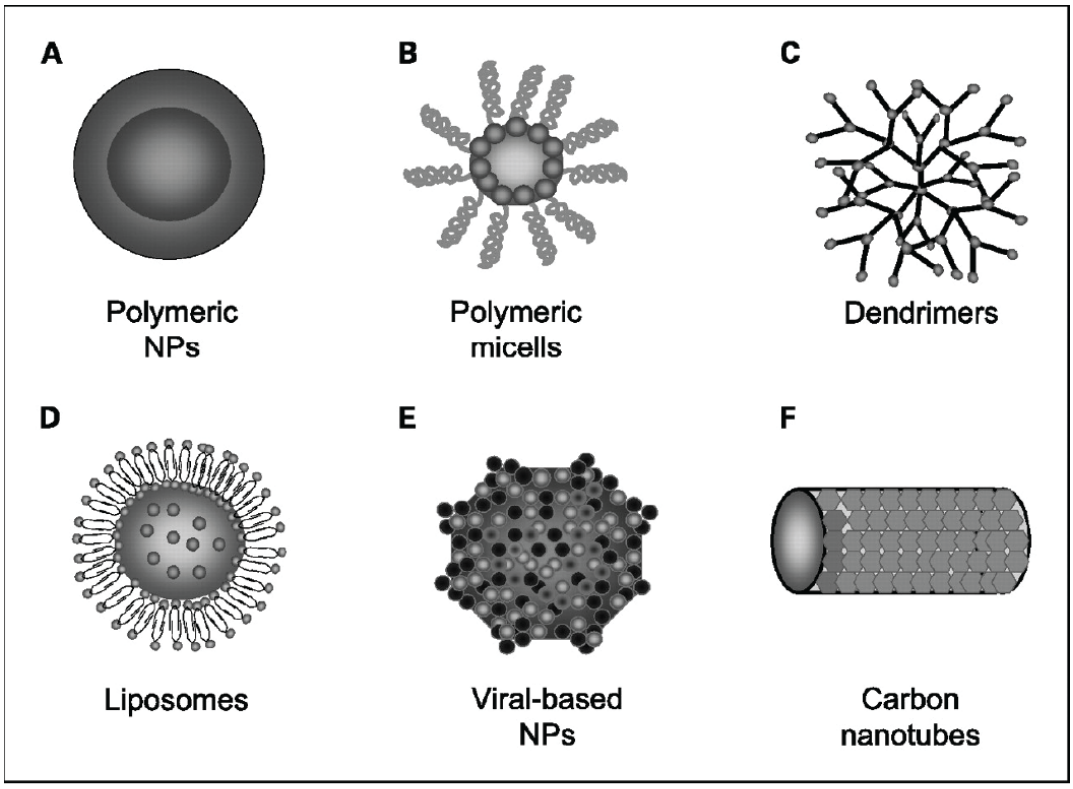

Figure 1: Nanoparticles have been developed for medical use using a wide variety of materials schemes. A, polymeric nanoparticles that are comprised of a polymerized carrying agent with a therapeutic or diagnostic agent entrapped in the polymer. B, Polymer micelles are formed by polymerizing a shell of material that is typically hydrophilic on one surface and hydrophobic on the other. The hydrophobic side typically interacts with an oil droplet that contains a hydrophobic drug. C, Dendrimers are large many branched hydrophilic polymers that contain binding domains throughout for holding therapeutic or diagnostic agents. D, Liposome's are formed with lipid bilayers that have a hydrophilic interior droplet containing the therapeutic agent while the outer surface is usually PEGylated. E, Viral based nanoparticles can either be generated by cells the secretet the virus nanoparticle, or by self assembly of the proteins in vitro into nanoparticles. F, Carbon nanotubes are long ~5μm grahphene tubes with diameters of ~5nm. They are hydrophobic, but can be functionalized with hydrophilic polymers, and can entrap hydrophobic drugs.

The MPS system

The arm of the immune system that is most commonly associated with nanoparticles is the reticuloendothelial system (RES)/mononuclear phagocyte system (MPS). The MPS system broadly consists of tissue macrophages and dendritic cells (DCs) found in the spleen, liver, and lungs as well as monocytes in the spleen and blood (Miyata and van Eeden, 2011; Moghimi et al., 2012; Wynn et al., 2013). In addition some authors have recently suggested that neutrophils in the blood should also be considered part of the MPS due to their similar function and behavior to other MPS cells, thoughtraditionally neutrophils have not been considered a part of the MPS system. The MPS system has been well characterized as functioning as the innate immune system's effecter arm in the blood (Fitrolaki et al., 2013; Kono et al., 2012; Ogiku et al., 2011). Additionally in pathological contexts the MPS system, especially the DCs, function as the main antigen presenting cells in the spleen for activation of adaptive T and B cell responses. This particular function will not be considered further here, but has been extensively reviewed recently (Blum et al., 2013; Fehres et al., 2013; Guery and Hugues, 2013).

In the liver kuppfer cells, tissue macrophages play a critical role under normal physiological conditions to remove microbes and microbial products from blood that enters the liver from the intestines (Crispe, 2009; Traeger et al., 2010). To facilitate this process, the kuppfer cells are found in the small liver sinusoids where blood flow is slow and the kuppfer cells project large numbers of filopodia

into the lumen of the blood vessel. When phagocytic receptors on the filopodia engage microbial surfaces the microbes are bound and rapidly internalized by the kuppfer cell, this process prevents bacteria and other microbes that commonly enter the blood in the intestines from passing into the rest of the body and causing sepsis (Gregory et al., 2002; Gregory and Wing, 2002; Shih-Ching et al., 2004; Wong et al., 2010). Kuppfer cells have also been implicated in a wide range of pathological conditions including liver fibrosis (Frasinariu et al., 2013; Purohit and Brenner, 2006; Tomita et al., 2013), fatty liver disease (Koek et al., 2011; Sawada et al., 2013), hepatic cancer (Bortolami et al., 2002; Van den Eynden et al., 2013), malaria (Frevert et al., 2008; Tavares et al., 2013a; Tavares et al., 2013b), and alcoholic liver disease(Bala et al., 2012; Petrasek et al., 2012; Szabo et al., 2012; Wan et al., 2013). If microbes are introduced directly into the blood, it is well known that the majority of microbes will be cleared by the action of kuppfer cells in the liver (Shou et al., 1994). In the case of genetic or pharmacolgical treatments which significantly blunt the activity of kuppfer cells there is a significantly increased risk of death during sepsis (Knoferl et al., 2002).

After the liver the second largest collection of MPS cells that access the blood is found in the spleen, where at least eight different distinct populations of macrophages can be found (den Haan and Kraal, 2012). The exact role and nature of all of the subpopulations of splenic macrophages is poorly understood, but most of the minor populations are believed to be important in antigen presentation (Randolph et al., 2008; Tacke et al., 2007). The most abundant type is the well-studied red pulp macrophage. Red pulp macrophages, as their name

implies, are located in the red pulp of the spleen. Under normal physiological conditions they remove aged red blood cells from blood as it passes through the spleen (Ganz, 2012). This action plays an important role in preventing anemia and inflammation from the lysis of aged red blood cells in inappropriate locations in the body (Kovtunovych et al., 2010). In the case of sepsis red pulp macrophages will bind and phagocytose microbes in the blood as it passes through the spleen. In the case of a normally functioning immune system the spleen will clear the second largest amount of microbes during sepsis after the liver, with the red pulp macrophage being the dominant player in this process.

The activity of macrophages in the lung is highly inconsistent from one species to another. All mammals contain large numbers of macrophages in the lungs, however in some species such as rodents (Fels and Cohn, 1986) the macrophages are polarized into the airways and do not respond to the presence of microbes in the blood of the lungs and therefore clear only small numbers of microbes during sepsis (Fels and Cohn, 1986). However in some larger mammals such as dogs, macrophages in the lungs appear to respond both to microbes in the airways and the blood allowing them to clear microbes in the case of sepsis (Merrill, 1990). Human lung macrophages appear to respond both to pathogens in blood and in the airways making the lung the third most prevalent site of clearance in humans after liver and spleen (Merrill, 1990).

Monocytes exist in the body in two distinct populations, CX3CR1 high and low. CX3CR1 high monocytes are found in the blood and peripheral blood

vessels under normal conditions where they appear to perform a patrolling surveillance function. In the case of injury CX3CR1 high monocytes quickly migrate into the site of injury where they first release cytokines and chemokines to draw other immune cells to the site of injury, then differentiate into tissue macrophages to assist in the clearance of invading microbes/cellular debris (Auffray et al., 2007; Geissmann et al., 2010). CX3CR1 low monocytes are normally resident in the spleen, but upon injury the chemokines during injury induces CX3CR1 monocytes to migrate from the spleen into the blood. After circulation in the blood they then enter the site of injury where they differentiate into macrophages (Swirski et al., 2009).

Neutrophils are the most prevalent immune cell in the body. They are generated at a constant high rate in the bone marrow, circulate in the blood for 18hrs-3 days, after which time they apoptose and are removed from the blood by macrophages in the spleen, liver and bone marrow (Maugeri et al., 2009). In the case of injury and/or infection neutrophils quickly enter the site of injury where they can act as phagocytes to remove pathogens, or in other circumstances release their granular contents of anti-microbial enzymes and reactive oxygen species in an attempt to kill invading pathogens (Pittman and Kubes, 2013). Other studies have shown neutrophils are important in the phagocytic clearance of activated platelets in blood, where they bind to and internalize platelets, and then transit to the liver, spleen or bone marrow to be phagocytically cleared by macrophages (Manfredi et al., 2010; Maugeri et al., 2012). Although neutrophils have long been known to be phagocytic they are often not grouped as part of the

MPS system likely due to their different life cycle and microbial killing activities. However, recently some authors have suggested that due to their lineage, motility and phagocytic capacity they should more properly be classified as an MPS cell (Rabinovitch, 1995; Silva and Correia-Neves, 2012). Surprisingly despite they abundance and phagocytic capacity few nanoparticle studies have examined their role in particle clearance. It has been shown however that certain particle types can be found in neutrophils after intravenous injection (Leuschner et al., 2011). In addition it has been shown that *in vitro* nanoparticles can be phagocytosed by neutrophils and induce neutrophil netting, a process in which the nuclear contents of the neutrophils are mixed with the granular contents and then exocytosed to create a DNA, granular, extracellular, anti-microbial net (Bartneck et al., 2010).

MPS clearance of nanoparticles

Early studies of the PK of nanoparticles injected intravenously showed surprisingly fast clearance of particles from the blood (Fernandez-Urrusuno et al., 1996). Upon further examination of the biodistribution (BD) of the particles it was shown that the majority of the particles were located within the kuppfer cells of the liver and the red pulp cells of the spleen (Illum and Davis, 1984; Illum et al., 1984). This result has subsequently been repeated with a wide variety of nanoforumlations with widely divergent physical and chemical characteristics (Zamboni et al., 2012). A large amount of research has been done examining the interactions between macrophages and nanoparticles *in vitro* to attempt to

indentify key factors involved in particle binding and clearance by macrophages. No study to date has been able to truly prevent all binding and clearance of particles, but several physical and chemical characteristics such as hydrophobicity, strong charge, rigidity, size, and the rate at which serum proteins bind to a particle have been identified as playing a negative role (Moselhy et al., 2000). From this work a general consensus has emerged that particles less than 500nm, that are flexible, hydrophilic and uncharged will demonstrate the best PK *in vivo*. Other studies have attempted to determine which specific receptors on macrophages bind to particles to mediate clearance. These studies have been primarily *in vitro* using immortalized cell lines, and often non-specific inhibitors with many characterized off target effects. These caveats make drawing any strong conclusions about important receptors difficult, but they do provide an initial list of suspects including scavenger receptor A (Patel et al., 2010), Fc gamma receptor three (Yang et al., 2010), compliment receptor 3 (Sahay et al., 2010), among others.

The most commonly used strategy to extend the circulation time of nanoparticles *in vivo* has been to graft a thick coating of high molecular weight polyethylene glycol (PEG) to the surface of particles. PEGylation works by providing a hydrophilic low charge surface that coordinates a shell of water molecules around the surface of the particle which slows the rate of protein adsorption to the particle (Owens and Peppas, 2006; Zamboni et al., 2012). PEG coating has been shown to significantly increase the circulation times and alter the BD of nanoparticles *in vivo* (Papahadjopoulos et al., 1991). However PEG does not

completely prevent clearance of particles by MPS cells, instead it slows the kinetics. In addition there are reasons to believe that PEG is a less than ideal solution for clinical applications. First it appears that PEGylation typically competes with targeting strategies as targeting molecules must protrude past the PEG layer and be present in sufficient quantities to result in targeting. This has a tendency to disrupt the coordinated shell of water around the particle, and creates the possibility of MPS cells binding directly to the targeting ligand, resulting in clearance (Pardeshi et al., 2012), or for serum proteins to bind to the particle opsinizing it. It has also been shown that a large number of patients treated with PEGylated agents will develop short term anti-PEG IgM antibodies (Ishihara et al., 2009; Shimizu et al., 2012), this response is transient, typically lasting for only a few weeks, but it significantly limits the flexibility of dosing schedules for PEGylated agents. In addition recent work has shown that as much as 25% of the population has circulating anti PEG IgG antibodies due to the presence of PEG in a large number of consumer products (Garay et al., 2012). While the combination of these factors suggests that PEG is not a sufficient solution for MPS clearance of nanoparticles, surprisingly little work has been done studying the biology of clearance, or coming up with alterative solutions to PEG for extending the circulation of nanoparticles.

Nanoparticle PK assays

The study of nanoparticle PK has typically utilized a blood draw assay in which nanoparticles are injected into a large number of animals at time zero. At various time points after injection the animals are sacrificed and bled. The collected blood can then be assayed for concentrations of nanoparticles by using reporters such as fluorescence or radiation (Zamboni et al., 2012). In the case of inorganic nanoparticles the concentration can be directly assayed by detecting the presence of elements in the particles not found in biological samples such as gold, in the case of gold nanoparticles or cadmium and selenium in the case of quantum dots (Dreaden et al., 2012a; Dreaden et al., 2012b). These assays are advantageous as they are simple to perform; the data can be applied to existing pharmacokinetic models for small molecule PK, and can provide direct concentrations of nanoparticles in blood and/or tissue. There are however several disadvantages to these assays: First this technique requires the use of large numbers of animals and therefore large amounts of nanoparticles, as a group of animals is required at every time point. Second these assays offer limited temporal resolution, it is difficult to get data points for less than 1-2min after injection of particles making the baseline value unclear, and every time point assayed requires the use of additional animals and particles. Third it is common for these types of experiments to result in high errors as it is difficult to sacrifice animals and bleed them in a controlled, repeatable way. These limitations make this type of assay unappealing for use when attempting to screen formulations of nanoparticles or animal models of disease due to the fact

that large numbers of often difficult to manufacture experimental particles or expensive/rare animals must be used. An alternate assay that allows for PK data from a small number of animals usingfewer particles and higher temporal resolution is critically needed by the field to allow for rapid screening of particles and animal models.

Intravital microscopy

Intravital microscopy is an emerging technique in biological sciences that allows for the direct imaging of cells, molecules, tissues, etc. in living animals. It is highly advantageous over traditional *in vitro* tissue culture based imaging for the obvious reason of being performed in a physiologically relevant system. Intravital microscopy is most commonly performed using a multiphoton microscope (Niesner and Hauser, 2011). This type of scope uses two carefully aligned infrared laser lines that cross at a precisely defined position. At the point where the two lasers cross their energy is roughly doubled allowing them to excite photophores that typically are excited by visible light (Benninger et al., 2008). This is advantageous as infrared light exhibits far greater tissue penetration than visible light allowing for the stimulation of photophores that would otherwise be too deep in tissue to be imaged (Bakalova, 2007). However, for imaging in tissues that are shallower such as the epidermis, it is often advantageous to use traditional laser scanning confocal microscopy as tissue penetration is less important and greater resolution can be achieved with traditional confocal microscopy. Intravital microscopy has been used recently to

study diverse biological processes including cancer invasion (Uchugonova et al., 2013), development (Canaria and Lansford, 2010), immune function (Sumen et al., 2004), neurobiology (Garaschuk et al., 2006), as well as many others. In nanomedicine intravital microscopy is slowly gaining traction and has recently been used to assay the effect of size and shape on tumor extravasation of particles (Smith et al., 2012), targeting of particles to neovasculature (Smith et al., 2008), the circulation of gold nanoparticles (Tong et al., 2009b), and the uptake of particles by tumors (Smith et al., 2010). By combining the knowledge and resources for intravital imaging of the immune system with intravital imaging of nanoparticles, we may be able to better understand the clearance of nanoparticles by the immune system. In addition, by directly imaging particle circulation in blood it is possible to use intravital microscopy as an alternative method for assaying nanoparticle circulation times that avoids many of the traditional complication of nanoparticle PK assays.

Th1/Th2 immunology

In recent years, the systems regulating the immune system and immune function have begun to be elucidated. At this point, the central cell controlling the immune network is known to be the CD4 positive (CD4+) T cell. These cells are the cornerstone of the adaptive immune system and serve as one of the major connection points between the innate and adaptive immune system (Schmitt and Williams, 2013). CD4+ T cells have no direct effector function on pathogens . However, upon stimulation with antigen and other co-stimulatory molecules

CD4+ T cells take on one of at least four different classes: the T helper cell, the Th1 T cell, the Th2 T cell, and the Th17 T cell (Boswell et al., 2011; Muranski and Restifo, 2013; Stadecker et al., 2004; Tundup et al., 2012). These populations are defined by the types of cytokines and chemokines that they secrete, and thereby inform other immune cell behavior. T helper cells are considered to be tolerogenic; they react to autoantigens and suppress the activity of CD8 killer T cells, and B cells that recognize the self antigen (Schmitt and Williams, 2013). They are characterized to secrete the cytokines interleukin 9 (IL-9), interleukin 10 (IL-10), and tissue growth factor beta (TGF-beta). Th1 T cells are typically elucidated by bacterial infections, they release interferon gamma (IFNg) as their primary effecter molecule (Cope et al., 2011). IFNg functions primarily to prime and activate cells of the innate immune system to fight microbial pathogens, by upregulating molecules required for the killing of bacteria and yeast. In addition, Th1 T cells contribute to inflammatory conditions in infected tissue, which allow for the entry of immune cells, the slowing of bacterial growth, and the influx of plasma carrying immune molecules such as antibodies and complement (Paulnock, 1992; Wynn et al., 1992). Macrophages activated by Th1 T cells are termed M1 or classically activated macrophages (Novak and Koh, 2013). Th2 cells are classically thought of to be induced by parasitic infections (Pearce and Reiner, 1995). They release TGF-beta, IL-4, IL-7 and IL-13 as effector molecules. These molecules stimulate the division and activation of cells involved in the elimination of parasites such as eosinophils and basophils, as well as promote a robust antibody response from B cells (Pulendran and Artis, 2012).

Macrophages activated by Th2 T cells are termed M2 macrophages (Mantovani et al., 2002). Th17 T cells are most classically thought of as being elucidated by viral infections (Romagnani, 2008), and have also been shown to mediate many autoimmune diseases (Brembilla and Chizzolini, 2012). IL-17 is the primary cytokine of Th17 cells. IL-17 strongly induces the actively of CD8 killer T cells to fight viral pathogens.

It is known that in humans exposure to certain types of infections early in life will have a tendency to polarize the immune system more towards one of these types of CD4+ T cell programs. This polarization will, in turn, cause an individual to be better protected from some types of pathologies and be more vulnerable to others (Grogan and Locksley, 2002). Despite the fact that these types of immune priming events are critical for immune function, nothing is currently known as to how CD4+ T cell priming affects the clearance of nanoparticles by the immune system. Fortunately, this is a tractable problem due to the fact that several laboratory mouse strains are known to naturally polarize towards one type of immune response or another. For instance, the strain C57BL/6 has been shown to always have a Th1 type immune response, while the strain BALB/c always has a Th2 type response (Mills et al., 2000).

M1/M2 Macrophages

In recent years, studies of macrophages have determined that based on the cytokine environment present, macrophages can polarize into at least two distinct phenotypes (Mills et al., 2000). The cytokines produced by Th1 CD4+ T

cells, primarily IFNg have long be known to induce a state of macrophage activation that is now known as classical or M1 activation (Nakano et al., 2001). In this case, macrophages are prepared for defense of tissue from invading microbes such as bacteria and fungi. To accomplish this, macrophages alter their morphology to become mesenchymal and upregulate enzymes involved in the formation of reactive oxygen species (ROS) such as nitric oxide synthase (iNOS) and microbial killing enzymes such as granzyme (Mills et al., 2000). Studies have shown that M1 polarized macrophages are more successful at both phagocytosing bacteria, and killing both phagocytosed bacteria and bacteria in surrounding tissue. M1 macrophages also secrete pro-inflammatory cytokines and chemokines to draw other immune cells to site of infection and activate them (Martinez et al., 2006). These effects render M1 macrophages highly effective at the elimination of invading microbes, but are also highly destructive to the surrounding tissue due to the high levels of inflammation they induce and direct damage from ROS (Nishio et al., 2005). More recently, it has been discovered that cytokines produced by Th2 immune responses also elucidate an activated state in macrophages, but with very different characteristics; these are known as alternatively activated or M2 macrophages (Mantovani et al., 2002; Tugal et al., 2013). M2 macrophages are thought to be involved primarily in the resolution of inflammation and tissue/wound repair (Mills et al., 2000). M2 macrophages maintain the standard macrophage amoeboid morphology allowing them to be more motile in tissue. They downregulate ROS producing enzymes such as iNOS and instead upregulate arginase, thereby preventing metabolism of

arginine to NO. In addition, a wide range of scavenger and lectin receptors are upregulated likely to help with the removal of microbial and cellular debris (Noel et al., 2004). Likely due to the upregulation of these receptors, M2 macrophages have been shown to more readily phagocytose oxidized low density lipoproteins, apoptotic bodies, and latex beads (Chinetti-Gbaguidi et al., 2011; Durafourt et al., 2012). Finally, M2 macrophages have been shown to secrete anti-inflammatory cytokines and induce division of tissue cells for the repair of injury (Cudejko et al., 2011).

The current model of infection suggests that macrophage function is a two-step process. Initially, macrophages present at the site of infection or monocytes recruited to the site of infection differentiate and/or polarize into M1 macrophages to fight microbes present at the infection. However, as runaway inflammation is highly damaging to the tissue after a certain length of time, M1 macrophages either repolarize to or are replaced by M2 macrophages. The M2 macrophages then function to remove cellular and microbial debris and to promote tissue growth and repair (Biswas et al., 2012).

Despite the marked difference in macrophage behavior between M1 and M2 macrophages and the fact that macrophages are a key player in the clearance of nanoparticles *in vivo*, no one has examined the effect of M1 vs. M2 polarization on nanoparticle clearance.

CHAPTER TWO: AN INTRAVITAL MICROSCOPY ASSAY FOR ASSESING THE RELATIVE PHARMACOKINETICS OF NANOPARTICLES *IN VIVO*

As discussed in chapter 1, the majority of PK assays for nanoparticles rely on a system of blood draws from multiple mice at certain defined timepoints to generate concentration of particles in blood over time. These assays are limited in their temporal resolution, error measurements, and repeatability due to the large number of mice required. For instance, using a fairly minimal number of time points for PK (control, 5min, 15min, 30min, 1hr, 2hr, 6hr, 12hr, 24hr) and a minimal number of mice (3 per time point), a blood draw PK experiment requires 27 mice for completion. Using a low dose of particles (15mg/kg) in an average weight young female mouse (20g) ends up requiring ~8mg of particles to be synthesized. For a better dataset that is more likely to reveal significant differences in particle PK, mouse and particle numbers will need to increase by at least 50%. This high requirement for numbers of mice and particles becomes extremely demanding on resources and time, especially when using difficult-to-synthesize experimental particles and/or difficult to maintain mouse models. Therefore, traditional blood draw PK assays are an unappealing method for screening various formulations of nanoparticles and/or mouse models of diseases or genetic manipulations. A better-functioning assay would involve the use of fewer mice (ideally less than 10), and therefore fewer particles, have high temporal resolution and low error, and be able to be completed in a short time

frame. This chapter will be devoted to describing the development of a novel intravital microscopy assay for nanoparticle circulation times *in vivo* that addresses the above needs. A description of this assay has been published in PNAS by Merkel et. al. (REF).

Detailed protocol: These assays were performed using an Olympus IV100 laser scanning intravital microscope. However, in principle this assay could be performed with limited modifications with any fluorescence microscope capable of supporting a heating pad during imaging.

Mouse preparation: Experiments were performed on young healthy female BALB/c mice with an average weight of 20g. Mice were prepared by anesthetization with inhalable isoflurane gas at 2% in O_2. Once mice were fully anesthetized, a pediatrics 27 gauge catheter was inserted into the tail vein and immobilized with superglue. The ear of the mouse was prepared by application of men's Nair to the ear for 1min, followed by washing the ear 4X with room temp water to remove all Nair and clean the ear. The mouse's ear was than observed for ~2min for any signs of irritation or inflammation from the Nair such as excessive redness especially around the blood vessels, swelling, or peeling of skin. If any of these were observed, the mouse was returned to the cage for future use. If no inflammation was observed, the mouse was carefully moved to the stage of the IV100 scope with care taken to not disturb the catheter. On the stage of the scope, the mouse's face was placed in a nose cone which delivered 2% isoflurane gas continuously. The heating pad on the stage was set to 37C and the ear was immobilized using two-sided tape on an aluminum block by

placing the outer edge of the ear on the tape, and then gently rolling a finger over the ear from the outer edge towards the head to flatten the ear. It is important to spread the ear from the outer edge in as going the other direction can result in burst capillaries at the outer edge of the ear and inflammation. If at any point in the process inflammation is observed in the ear, the experiment should be stopped as inflammation results in particles accumulating in the site of the inflammation and, therefore. gives false PK data.

Imaging setup: Blood vessels were located in the mouse's ear by illuminating the ear with white light and then imaging with the green fluorescence channel (excitation 488nm, short pass filter 506-540nm). The 506-540nm component of the white light was reflected off of tissue in the mouse ear to produce a bright signal, while the hemoglobin in the blood vessels absorbs light in those wavelengths resulting in dark regions where blood vessels are located (Figure 1 A).

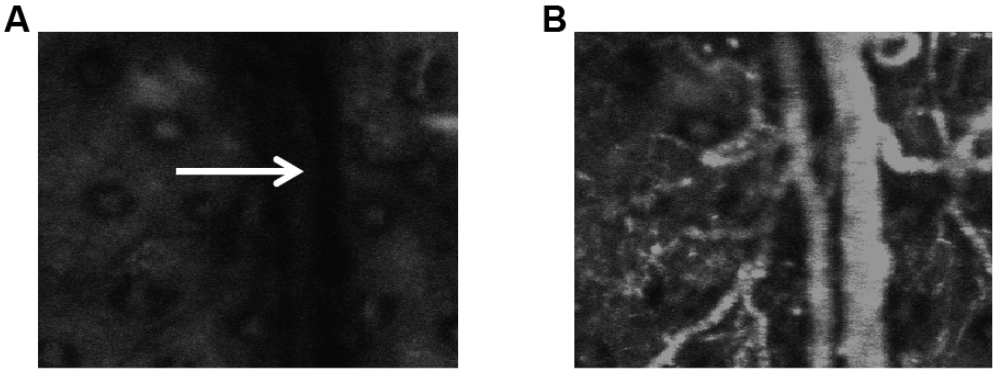

Figure 2: Images of vasculuture in mouse ear. Pannel A shows the ear illuminated with white light and imaged in the green florescence channel. The white arrow marks the location of the blood vessel that can be seen by the dark region in the otherwise bright field of autoflorescence. Pannel B shows the same region affter injection with Alex 647 labeled BSA and imaging in the far red channel.

In initial experiments the location of vessels was confirmed by injection of vascular contrast agents such as BSA conjugated to Alexa647 dyes (Figure 1 B). After blood vessels were located, the scope was set to image under the same protocol that would be used for particles (example, 1 frame/sec, 70% 633 laser, PMT gain 700, offset 0, dwell time 10µs/pixel, 320X320 pixels) for 15 min. After 15 min the movie was examined for evidence of significant drift in the XY or Z dimensions. If drift was observed the ear would be removed from the block, and a fresh piece of tape placed on the block followed by retaping the ear and another 15min imaging. When the ear was shown to be stable we proceeded to the particle imaging.

Particle imaging: For initial experiments developing this intravital microscopy assay we used PRINT® microparticles, utilizing the PRINT system as described (ref). Imaging sessions lasted 2hrs with frames being acquired every 5sec throughout. Before injecting particles blood vessels were located with atofluorescence or fluorescent BSA (Fig 2 A). Four frames were acquired

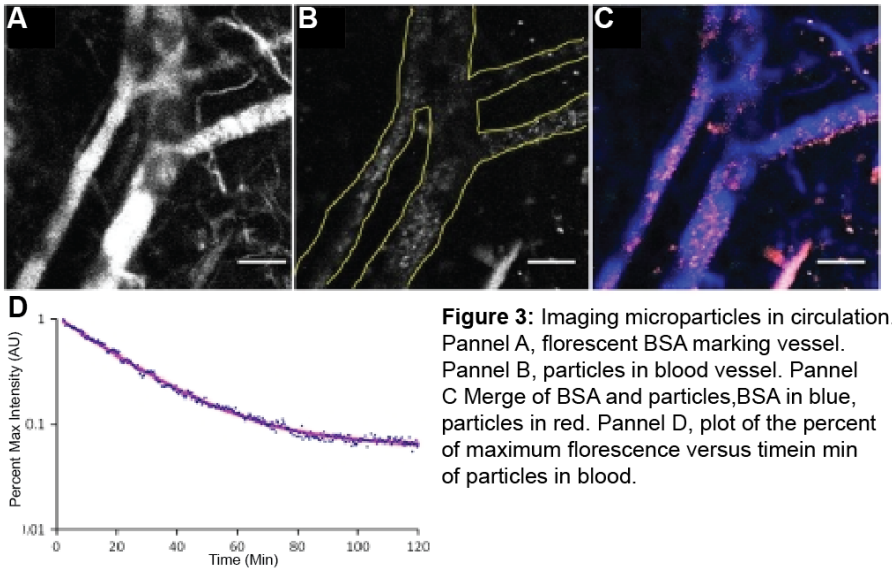

Figure 3: Imaging microparticles in circulation. Pannel A, florescent BSA marking vessel. Pannel B, particles in blood vessel. Pannel C Merge of BSA and particles,BSA in blue, particles in red. Pannel D, plot of the percent of maximum florescence versus timein min of particles in blood.

prior to particle injection in the far red channel to serve as a baseline reading for particle intensity. 500µg of particles were then injected followed by flushing the catheter with 40µl of heparin lock solution. The particles quickly filled the blood vessel and were visualized by the scope (Fig 2 B and C). Throughout the course of the imaging the number of circulating particles decreased as expected (Fig 2 D). To examine if the assay showed differences in circulation times for microparticles of different stiffness, as would be expected, we dosed mice with four different particle types with Young's modulus's ranging from 63.9kPa to 7.8kPa.

Image analysis: Movies were exported as TIF files to ImageJ for analysis. In ImageJ individual TIFs were complied together into stacks. Each stack was condensed by averaging four frames together using the intensity projection plugin. This resulted in 360 frames over 2hrs, or one frame for every 20sec. A straight line region of interest (ROI) was drawn in the main vein present in each movie. The average fluorescent intensity in the ROI was calculated for each frame of the movie. This data was exported to Microsoft Excel or GraphPad Prism for further analysis. Analysis included calculating lines and area under the curve to compare circulation times between particles of different modulus, or deriving PK values such as particle T1 and T2 half-lives and elimination volumes (Table 1). Analysis revealed that as expected decrees in particle modulus resulted in increases in particle circulation times.

TABLE 1.

Modulus values and compartmental analysis of RBCM particles from intravital microscopy experiments

% Cross-linker	Modulus of bulk material, kPa	Distribution half-life, h	Elimination half-life, h	AUC, fluoresence* h	Average R^2
10%	63.9 ± 15.7	0.038 ± 0.0012	2.88 ± 0.92	0.65 ± 0.14	0.8966
5%	39.6 ± 10.4	0.066 ± 0.036	5.12 ± 2.17	0.76 ± 0.57	0.9029
2%	16.9 ± 1.7	0.15 ± 0.025	7.12 ± 0.82	1.35 ± 0.26	0.9468
1%	7.8 ± 1.0	0.35 ± 0.13	93.29 ± 31.09	15.44 ± 15.63	0.9330

*Ranges given represent one standard deviation. Values were derived from scans of three mice.

Confirmation of intravital results: To confirm that the new intravital PK assay was delivering valid results, we re-tested the results from with the 1% crosslinker using a traditional blood draw PK. A large number of mice were injected with 500µg particles at the beginning of the experiment. Four mice were sacrificed at 5min, 30min, 1hr, 2hrs, 12hrs, 24hrs, 48hr, 138hrs post injection. Mice were sacrificed by cardiac puncture and the blood and organs were collected. The fluorescence intensity in the blood was calculated for each time point and the PK values for the micro particles were derived from these measurements (Table 2). No statistical difference was observed between the data set from the intravital PK and traditional blood draw PK experiments.

TABLE 2.

Pharmacokinetic parameters for 1% cross-linked RBCMs calculated from blood draws taken out to 5 d postinjection

A, mg/mL	B, mg/mL	α, h^{-1}	β, h^{-1}	$\alpha t_{1/2}$, h	$\beta t_{1/2}$, h	V_C, mL	AUC, mg · h/mL	CL_T, mL/h	Vd_β, mL
0.190	0.0482	0.241	0.00768	2.876	90.235	2.934	7.067	0.0990	12.894

CHAPTER THREE: THE EFFECT OF TH1 AND TH2 IMMUNITY AND MOUSE STRAIN ON NANOPARTICLE CLEARANCE

INTRODUCTION:

The potential clinical applications of nanoparticles and nanoformulations have been investigated for more than 30 years. Nanoparticle approaches have the potential to revolutionize drug delivery by allowing for the encapsulation of drugs with poor solubility or stability in a stable carrier particle. In addition, targeting nanoparticles to specific pathological sites may allow increased effective dose of drug at the needed site while decreasing systemic drug exposure, and therefore side effects. However, to date, only two nanoformulations for cancer treatment have been approved for clinical use (Doxil and Abraxane) (Coleman et al., 2006; Gradishar, 2006b; Krown et al., 2004). One major obstacle for the use of nanoparticles in vivo is rapid clearance by the cells of the reticuloendothelial system (RES)/ mononuclear phagocyte system (MPS) (Alexis et al., 2008; Leuschner et al., 2011; Nel et al., 2009; Zamboni et al., 2012). In addition to rapid clearance, variable activity of the MPS between patients leads to widely variable pharmacokinetics of nanoformulations in the clinic, reducing the efficacy of both approved and future experimental nanoformulations (Zamboni et al., 2009). The main strategy for extending the circulation time of nanoparticles is grafting of uncharged hydrophilic polymers onto the surface of particles for “stealthing”, with the most common polymer used being polyethylene glycol (PEG) (Owens and Peppas, 2006). PEGylation of

particles clearly extends their circulation time in vivo (Papahadjopoulos et al., 1991; Zamboni et al., 2012); however, up to 25% of patients exhibit circulating anti-PEG antibodies prior to treatment, or develop anti-PEG antibodies after the first administration of PEGylated particles (Garay et al., 2012; Shimizu et al., 2012). These factors limit the utility of PEGylation of nanoparticles in the clinic and suggest that a better understanding of the biomolecular interactions of nanoparticles and the MPS is critical for the development of alternative methods to PEGylation for the extension of nanoparticle circulation times in vivo.

The MPS is comprised of the macrophages and dendritic cells located in the liver and spleen, as well as monocytes and other phagocytic cells in the blood and spleen. When nanoparticles are injected intravenously and begin to circulate in the blood, they make direct contact with these MPS cells. Once a particle is in contact with MPS cells, receptors on the cell surface either directly recognize the particle, or recognize opsonizing serum proteins that have become attached to the particle. This leads to internalization of the particle and sequestration in the MPS cells (Yoo et al., 2010). Extensive work has been done to understand particle uptake at the cellular level, with various studies implicating scavenger receptors (Patel et al., 2010), complement (Yang et al., 2010), and Fc receptors (Sahay et al., 2010). The majority of these studies have been conducted with immortalized macrophage cell lines in vitro, and with various types and sizes of particles. However, the physiological relevance of particle uptake by immortalized cell lines in vitro for clearance in vivo is unclear.

Another relevant factor that has received little attention in the nanoparticle field is the effect that global immune status, such as the balance of Th1/Th2 cytokines and M1/M2 macrophages, has on the clearance process. During immune responses, helper T cells adopt distinct Th1 or Th2 identities, leading to the secretion of specific combinations of cytokines and chemokines that instruct a wide variety of immune cells, including macrophages [as reviewed in Murphy et. al. (Murphy and Reiner, 2002)]. The presence of Th1 cytokines has a tendency to polarize macrophages towards a pro-inflammatory M1 phenotype (Mills et al., 2000). Conversely, Th2 immune responses can induce macrophage polarization towards an anti-inflammatory M2 phenotype that promotes wound healing and the resolution of inflammation, yet is known to contribute to diseases such as allergies and asthma (Gordon and Martinez, 2010; Mills et al., 2000). In addition, M1 and M2 macrophages express different repertoires of phagocytic receptors, and may show differential efficiency of endocytosis and phagocytosis (Gordon and Martinez, 2010; Mills et al., 2000). It appears the effect of macrophage polarization on phagocytosis is target-dependent: M1 macrophages show enhanced phagocytosis of *S. aureus (Krysko et al., 2011)*, while M2 macrophages are more phagocytic towards myelin (Durafourt et al., 2012), apoptotic cells, and latex beads (Chinetti-Gbaguidi et al., 2011). Development of T cell based immune responses requires days to weeks, and would not be immediately provoked by exposure to particles. However, it is possible that Th1/Th2 priming from previous immune responses or differences in genetic

background could affect clearance of nanoparticles via changes in the relative number of M1 vs. M2 macrophages (Murphy and Reiner, 2002).

Current techniques for assaying quantitative or relative nanoparticle pharmacokinetics (PK) have significant drawbacks for screening multiple particle types and/or animal models due to issues with time, expense, sensitivity, and temporal resolution (see Discussion). Intravital microscopy (IVM) is an appealing alternative for assaying relative PK of nanoparticles in vivo. IVM has been used to assay the accumulation of targeted particles in tumors (Smith et al., 2008), tissue (Hak et al., 2010), the circulation time of gold nanorods (Tong et al., 2009a), the accumulation of particles in the liver (Cheng et al., 2012), the effect of size and shape on tumor extravasation (Smith et al., 2012) and the circulation of hydrogel microparticles (Merkel et al., 2011). In order to determine the roles of particle parameters and global immune status on nanoparticle PK, a calibration quality nanoparticle that has low batch-to-batch variability, with very low polydispersity is required. To this end, we used the Particle Replication in Non Wetting Templates (PRINT®) technique to generate particles of varying sizes. PRINT provides superior control over particle geometry and physical properties by taking advantage of a novel soft lithography technique for particle fabrication. This results in low batch-to-batch variability while having very low polydispersity values (Rolland et al., 2005) (Gratton et al., 2008b). Recent work has demonstrated that the PK of PRINT nanoparticles can be carefully and

reproducibly calibrated by adjusting the density of PEG chains present on the surface (Perry et al., 2012).

In this study, we observed striking differences in nanoparticle clearance kinetics between commonly used ‘wild-type’ mouse strains using intravital microscopy and flow cytometry. We have identified the cell types and anatomical locations of this differential clearance and identified the global (Th1 vs. Th2) immune status as a critical factor in nanoparticle clearance in vivo.

RESULTS:

Intravital microscopy (IVM) allows for rapid screening of nanoparticle clearance.

The ability to easily and inexpensively screen different formulations of nanoparticles in animal models is an unmet need in the field of nanomedicine. To address this need, we have modified an intravital microscopy technique that we recently developed to measure the pharmacokinetics of red blood cell mimetic microparticles (RBCM) (Merkel et al., 2011). This technique allows for screening the relative nanoparticle resident times in the blood using as few as four animals per condition. In order to reduce variation in nanoparticles for these experiments, we have employed the PRINT technique to generate monodisperse 300 nm cylindrical PEG hydrogel nanoparticles containing far-red fluorescent dyes for in vivo and in vitro imaging (Fig. 5); these particles are similar in size and composition to those used in a recent study by our group (Perry et al., 2012). When injected intravenously (IV), these particles produce bright fluorescence in the vasculature of a mouse and can be easily imaged in the ear (Fig. 5A-C). A time vs. fluorescence intensity profile can then be generated, and the area under the curve (AUC) can be calculated (Fig. 5D). By comparing the AUC from different mice we can determine the relative exposure of nanoparticles to blood in vivo.

A

Particle	Size	PDI	Zeta (mV)
200nm PRINT cylinders	305.1nm	.066	-26.4
6µm PRINT microparticles	5.9µm	NA	-18.6
Qdots	32.1nm	.328	-37.8

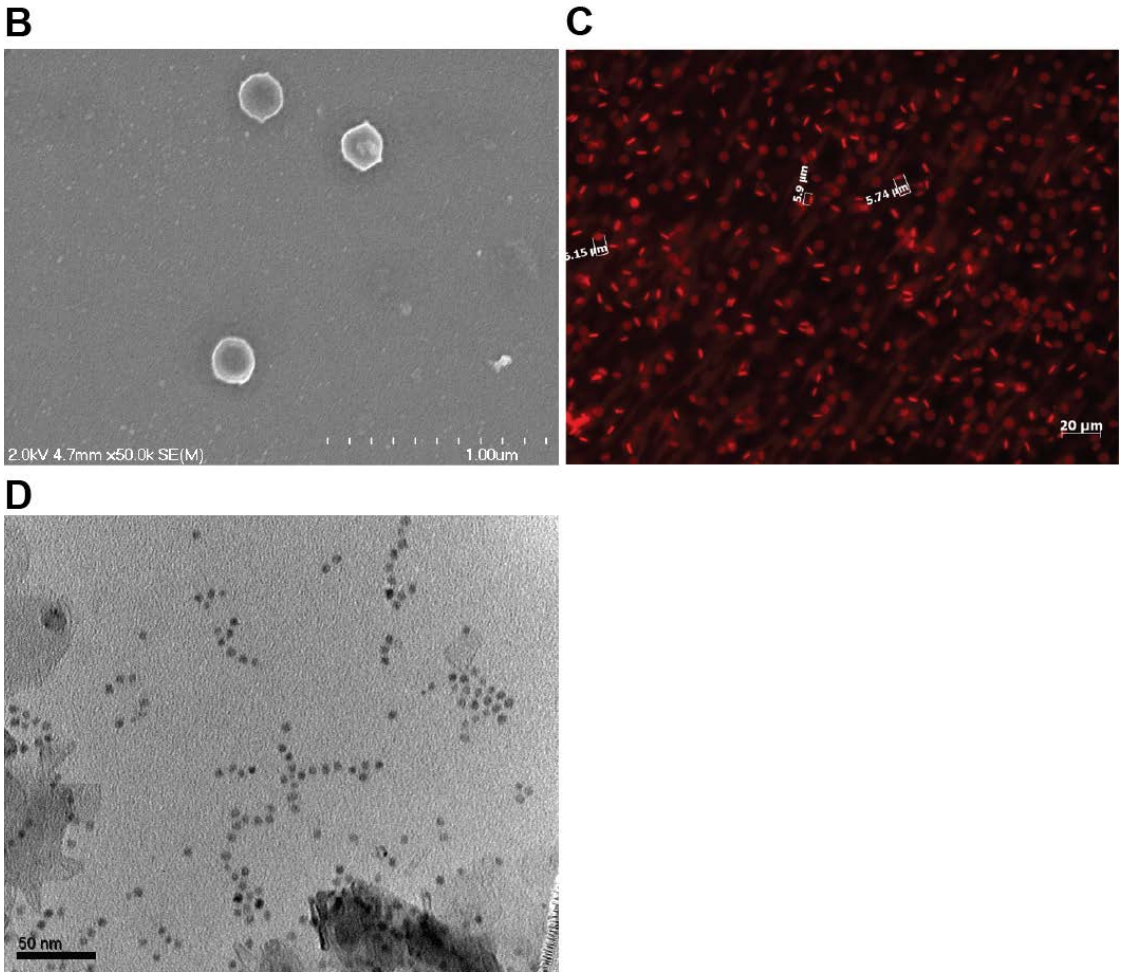

Figure 4: Characterization of particles used in experiments.

(A) Size, PDI, and Zeta potential for all particles used. Size was determined by dynamic light scattering for 200nm PRINT particles and Qdots, fluorescence microscopy was used to determine size of microparticles.

(B) Scanning electron micrograph of 200nm PRINT particles.

(C) Fluorescence microscopy image of microparticles scale bar is 20µm.

(D) TEM image of Qdots on glass scale bar is 50nm

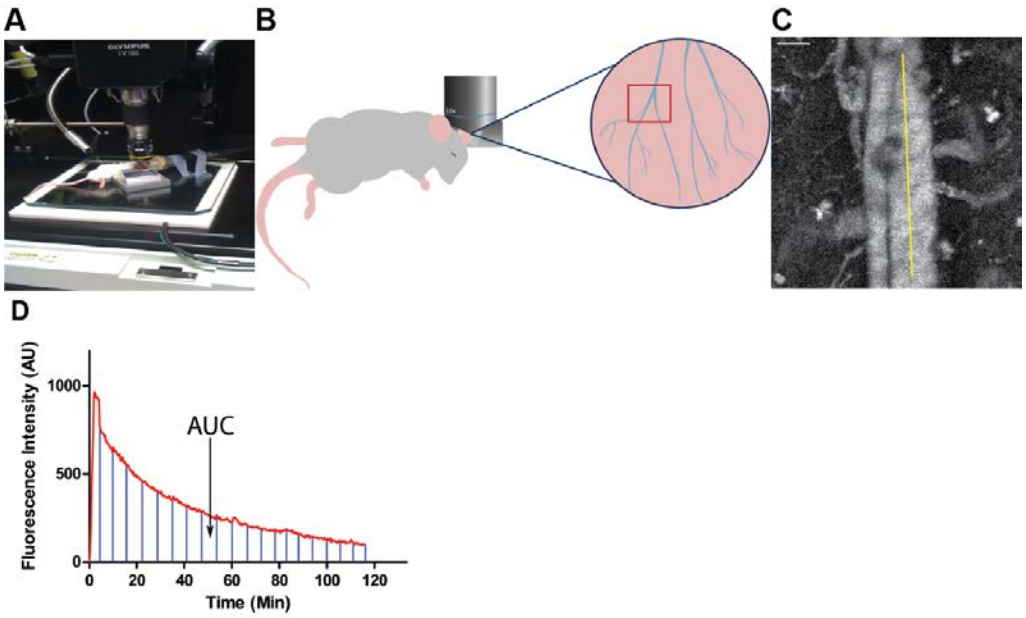

Figure 5: An Intravital Microscopy Based Assay for Screening Nanoparticle Clearance Rates in Live Animals

(A) A blood vessel is positioned in the center of the scan area.

(B) A cartoon showing the orientation of the mouse, the positioning of the objective, and the region of the mouse ear imaged.

(C) Movies are analyzed in ImageJ by selecting a straight line ROI in the large vein and average fluorescence intensity for each time point is calculated. Scale bar equals 50µm.

(D) A representative fluorescence vs. time plot of nanoparticle clearance. Marked region represents the area under the curve, which is calculated to determine relative exposure to blood for particles.

As the clearance of nanoparticles is mediated by the phagocytic cells of the mononuclear phagocyte system (MPS), we depleted these cells from female BALB/c mice using liposomal clodronate (Clod) (Camilleri et al., 1995) and continuously measured the blood fluorescence over a two hour period in treated and untreated mice (Fig. 6A). As expected, plots of average fluorescence intensity over time show a greater peak fluorescence intensity and longer nanoparticle residency in blood for Clod- treated mice compared to untreated controls (Fig. 6B). To compare the relative exposure of nanoparticles to blood between the two conditions, the area under the curve was calculated (Fig. 6C) and showed a >6-fold increase of particle exposure to blood in Clod-treated mice. This experiment validated that IVM can be used to screen relative exposure of nanoparticles to blood.

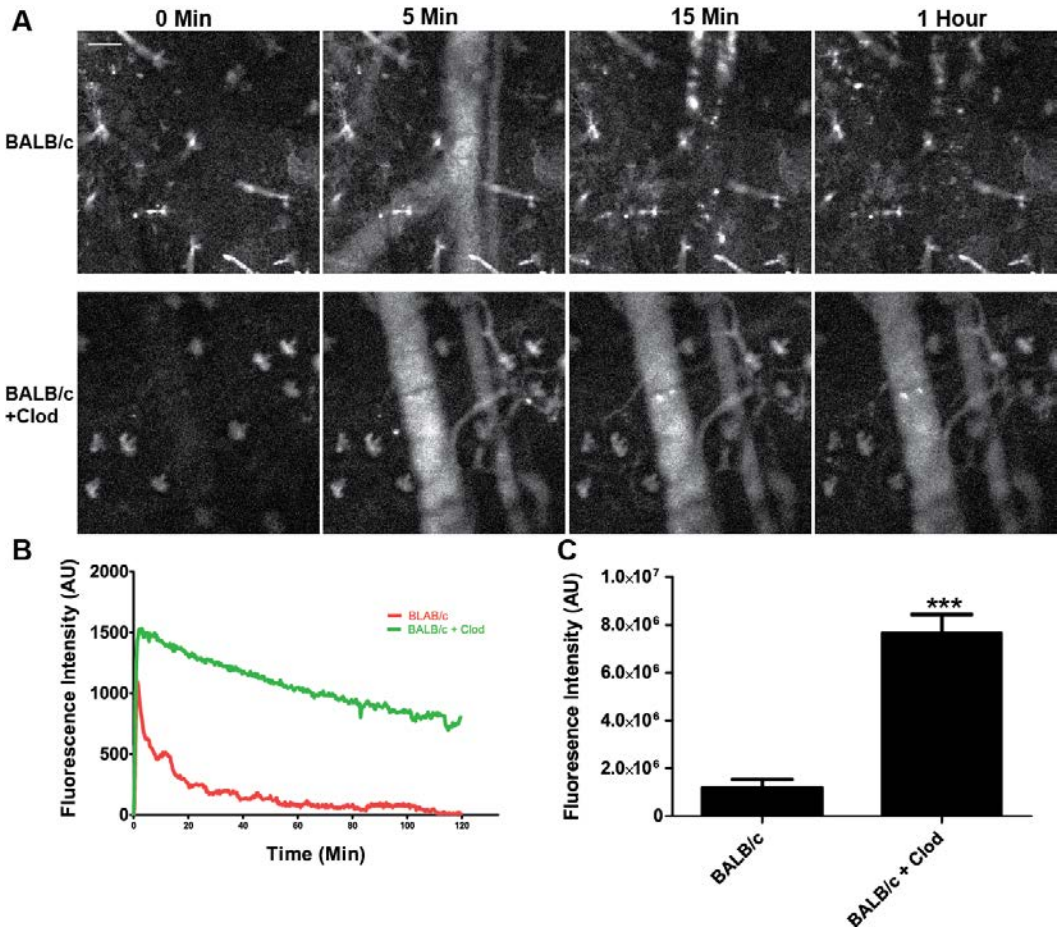

Figure 6: Treatment of BALB/c mice with liposomal clodronate increases the circulation of nanoparticles *in vivo*.

(A) Still images from a BALB/c mouse and a BALB/c mouse pre-treated with liposomal clodronate show significant differences in blood fluorescence from nanoparticles. Scale bar equals 50μm.

(B) A plot of mean fluorescence intensity versus time shows the difference in particle clearance rates between the two conditions (N=4).

(C) Plotting area under the curve shows a significant ($p<0.003$, t test) increase in fluorescence intensity in blood with clodronate pretreatment (N=4).

Interestingly, we observed that in all BALB/c mice after a significant fraction of the particle dose had been cleared from the blood, areas containing

concentrated particles became visible. Upon careful observation, it became clear that these visible areas of fluorescence were cells and not extracellular aggregates of particles, as some of them moved in a random manner including some periods of persistent migration against the blood flow (Fig. 7). Based on observations from others, it is likely that these cells are a combination of neutrophils and peripheral monocytes (Auffray et al., 2007). This uptake of particles in the peripheral vasculature could explain the common finding across many nanoparticle studies that a significant fraction of the injected particle dose is not recovered from the exsanguinated blood and major organs (Vasquez et al., 2011). Since a substantial proportion of blood vessel surface is left behind in the carcass and skin, particle clearance in the peripheral vasculature may account for some of the missing dose.

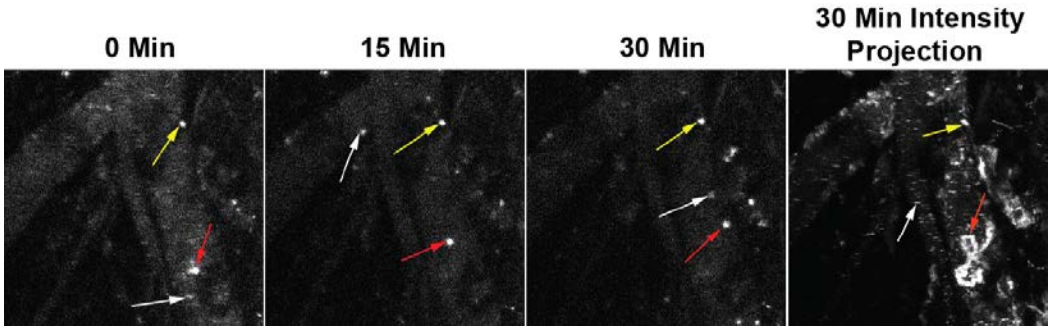

Figure 7: Peripheral immune cells clear nanoparticles in the vasculature.

Still images from representative movie (Sup. Movie 3) show the presence of three different types of cells made fluorescent by the uptake of labeled nanoparticles. White arrow indicates a cell that is free flowing in the blood and present for only a single frame of the movie, the red arrow shows a single randomly migrating cell and the yellow arrow shows a stationary cell. The 30 minute max intensity projection shows that the migrating cell (red arrow) moved through a circuitous route including migrating against the blood flow.

Different mouse strains clear nanoparticles with different kinetics.

The removal of nanoparticles from blood is mediated by the MPS system, and has been well studied on the cellular level by examining the role of various phagocytic receptors and endocytic/phagocytic mechanisms for particle uptake (Patel et al., 2010; Sahay et al., 2010; Yang et al., 2010). These properties of MPS cells are regulated at the level of the whole animal by higher order immune regulation mechanisms such as T-helper (Th) status(Martinez et al., 2006). However, the role of these global immune properties on nanoparticle clearance kinetics has been poorly studied. We examined the effect of Th1/Th2 immune priming in mice by measuring the blood exposure of nanoparticles in two Th1-biased mouse strains (C57BL/6 and B10D2 (Mills et al., 2000)), two Th2-biased mouse strains (BALB/c and DBA/2 (Mills et al., 2000)), as well as BALB/c and C57BL/6 mice treated with Clod (Fig 8A). We observed that nanoparticle blood exposure was significantly higher in Th1-biased strains than in Th2-biased strains (Fig 8B, C), suggesting that clearance mechanisms differ according to mouse strain. Clod treatment increased blood exposure in BALB/c, but not the C57BL/6 strain (Fig. 8B, C), indicating that little MPS-mediated clearance occurs in the first two hours for Th1-biased strains. In addition, we consistently observed that the initial peak fluorescence for BALB/c mice was significantly lower than in all other strains. Clod treatment resulted in BALB/c peak fluorescence levels similar to that of other strains, indicating that this lower peak fluorescence was

due to the MPS. As peripheral immune cells containing particles were consistently observed to a greater extent in BALB/c mice compared to other strains tested, it is possible that peripheral clearance is stronger in BALB/c mice resulting in a significant amount of particles being cleared in the first pass through the circulatory system.

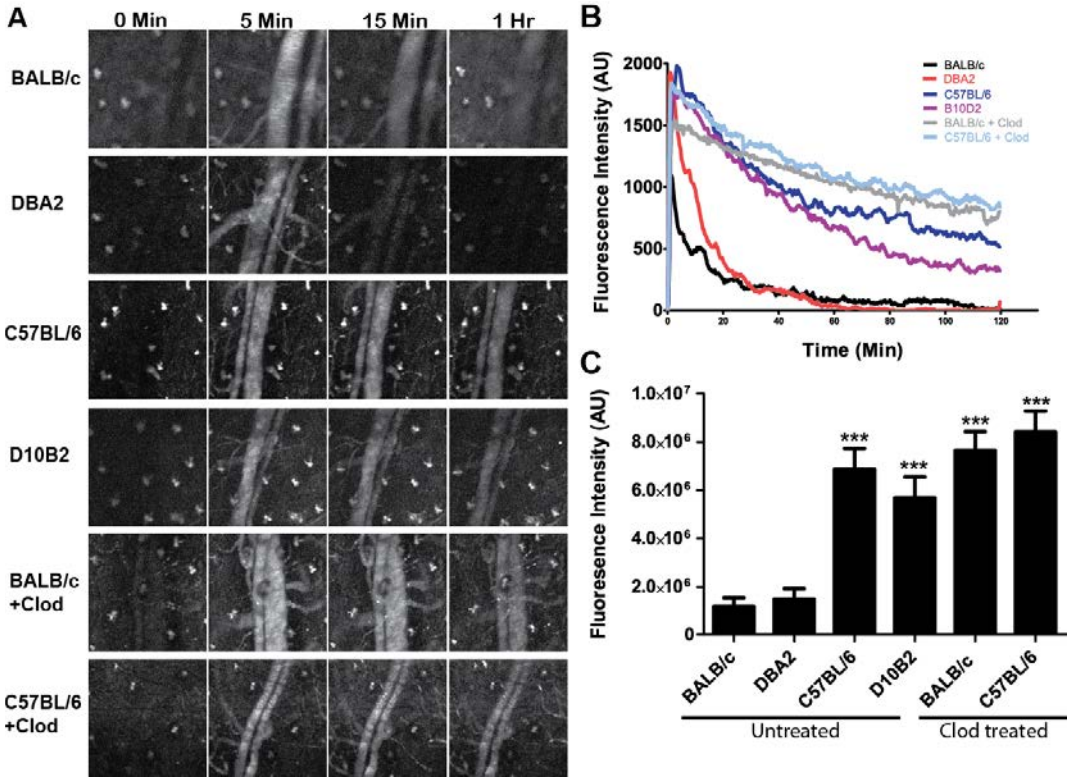

Figure 8: Th1 mouse strains clear nanoparticles slower than Th2 strains.

(A) Still images from supplemental movies 1-6 show the differences in particle circulation between the four mouse strains as well as liposomal clodronate pre-treated BALB/c and C57BL/6 mice.

(B) Plots of fluorescence intensity versus time for all four mouse strains and clodronate-treated mice (N=4 mice per condition).

(C) Plots of area under the curve for all conditions show a significant ($p<0.0001$, One-way ANOVA Dunnett post-test) increase in blood fluorescence between BALB/c and C57BL/6 and B10D2 mice, but not DBA2. Clodronate treatment significantly increases ($p<0.003$, t-test) blood fluorescence in BALB/c mice, but not C57BL/6.

To further address differences in clearance, we performed a biodistribution study by injecting BALB/c and C57BL/6 mice with particles and then sacrificing mice at 5min, 30min, 2hr and 24hrs post injection, followed by measuring fluorescence in homogenates of tissues by using a plate reader. Relative particle distribution was measured in the non-lymphoid organs (heart, lung, and kidneys (Fig. 9A)), lymphoid organs (spleen and liver (Fig. 9B)), whole blood (Fig. 9C), plasma (Fig. 9D), and blood cell fraction (red cells and leukocytes of whole blood) (Fig. 9E). Non-lymphoid organs showed low levels of particles at all time points, but C57BL/6 mice showed significantly higher levels of particles at 30min and 2hrs in heart and kidney, likely due to more particles still being present in blood contained in those organs. Spleen and liver showed a high level of particle uptake at all time points, with BALB/c mice having significantly more particles present at 5min, 30min and 2hrs. By 24hrs no significant differences were observed in any organ or compartment. Whole blood and plasma showed significantly more particles in C57BL/6 mice at 5min, 30min and 2hrs, but no significant difference was present by 24hrs. Blood cells showed significantly more particles in BALB/c mice at 5min and 30min, consistent with the IVM results.

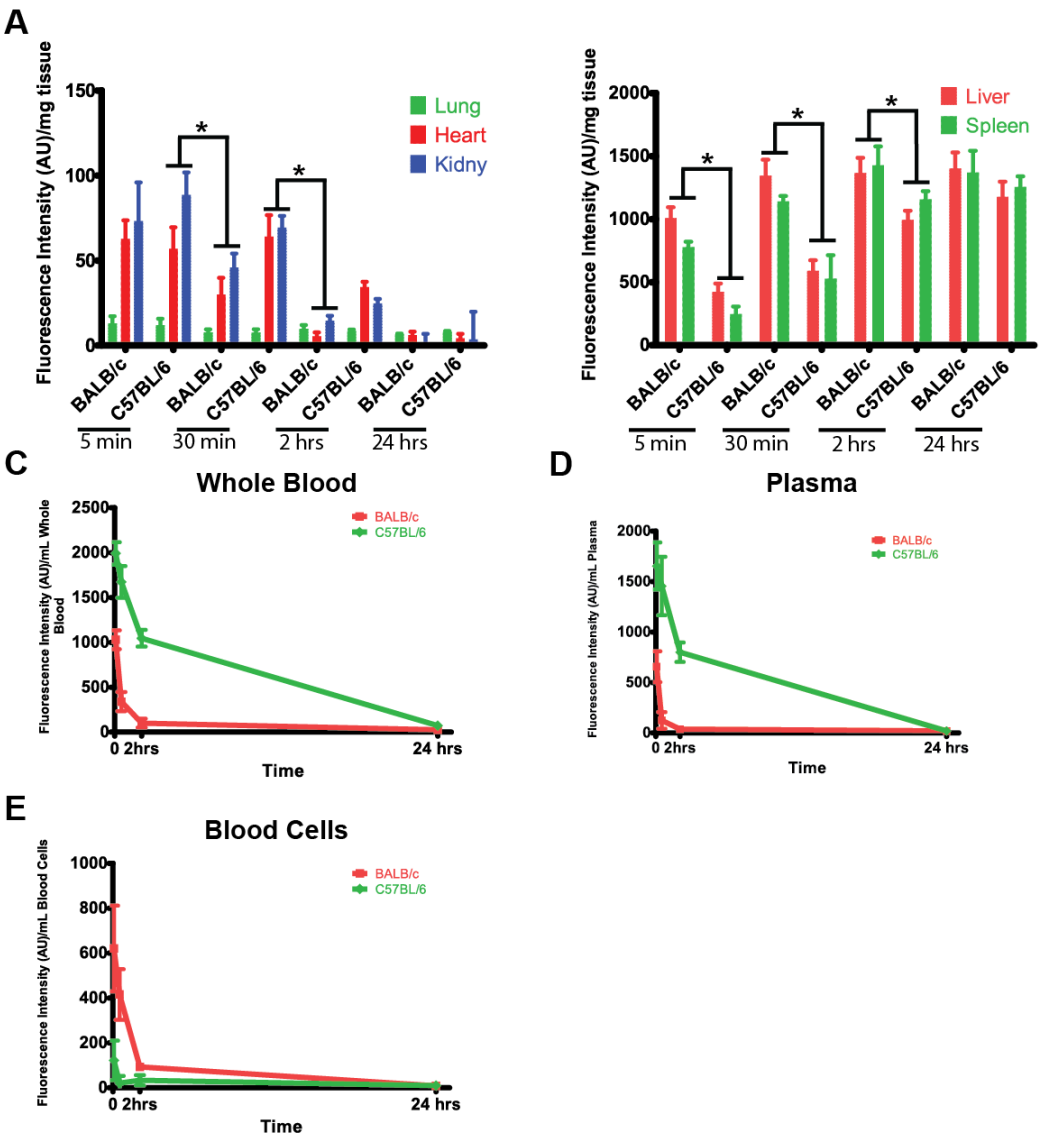

Figure 9: Biodistribution of 300nm PRINT hydrogel particles in Balb/c and C57BL/6 mice.

(A) Distribution of particles in the lungs, heart, and kidneys of Balb/c and C57BL/6 mice. C57BL/6 mice showed significantly higher amounts of particle in heart and kidneys then Balb/c mice at 30min ($P<.05$ t-test), and 2hrs ($P<.004$ t-test) (N=4).

(B) Distribution of particles in the liver and spleen of Balb/c and C57BL/6 mice. C57BL/6 mice showed significantly lower amounts of particle present in both liver and spleen compared to Balb/c mice at 5min, 30min and 2hrs ($P<.05$ t-test) (N=4).

(C) Relative amounts of particle present in Balb/c and C57BL/6 whole blood, C57BL/6 had significantly higher levels of particles in blood at 5min, 30min and 2hrs compared to Balb/C mice (P<.05 t-test) (N=4).

(D) Relative amounts of particle present in Balb/c and C57BL/6 plasma, C57BL/6 had significantly higher levels of particles in blood at 5min, 30min and 2hrs compared to Balb/C mice (P<.05 t-test) (N=4).

(E) Relative amounts of particle present in Balb/c and C57BL/6 blood cell fraction of whole blood, C57BL/6 had significantly higher lower of particles in blood at 5min, and 30min compared to Balb/C mice (P<.05 t-test) (N=4).

Some of the differential clearance of particles is due to uptake by granulocytes in Th2 prone strains.

To further understand the differences in clearance of nanoparticles by Th1 and Th2 prone mouse strains, we performed flow cytometry analysis of BALB/c and C57BL/6 peripheral blood leucocytes (PBL), splenocytes, and lymph nodes at 2hrs post injection. Lymph nodes were also assayed at 24hrs post injection to check for trafficking of phagocytes with particles to lymph nodes. We utilized a multi-marker flow cytometry protocol to determine particle uptake by lymphocytes (T and B cells), macrophages, monocytes, granulocytes, and dendritic cells (DC's) (Fig, 10). Lymph nodes showed no particles present at 2hrs or 24hrs post injection (data not shown), suggesting that the PRINT particles used do not gain access to the lymphatic system after IV injection. Uptake by T and B cells was minimal in both strains at 2hrs in blood and spleen, with no significant difference between strains (Fig. 11A). Uptake by DC's was observed in the spleen in both strains at 2hrs, with C57BL/6 DC's showing a significantly lower percentage of positive cells (Fig. 11B). Uptake by tissue macrophages (fully differentiated monocytes defined by the marker F480) showed no significant difference

between strains in the spleen (Fig. 11B). Surprisingly, uptake by monocytes in blood and spleen was significantly higher in C57BL/6 mice (Fig. 11A,B), but uptake by granulocytes was dramatically lower in both blood and spleen in C57BL/6 mice (Fig. 11A,B). These data suggest that some of the differential clearance observed between these mouse strains may be due to differential utilization of monocytes vs. granulocytes for particle uptake in the blood.

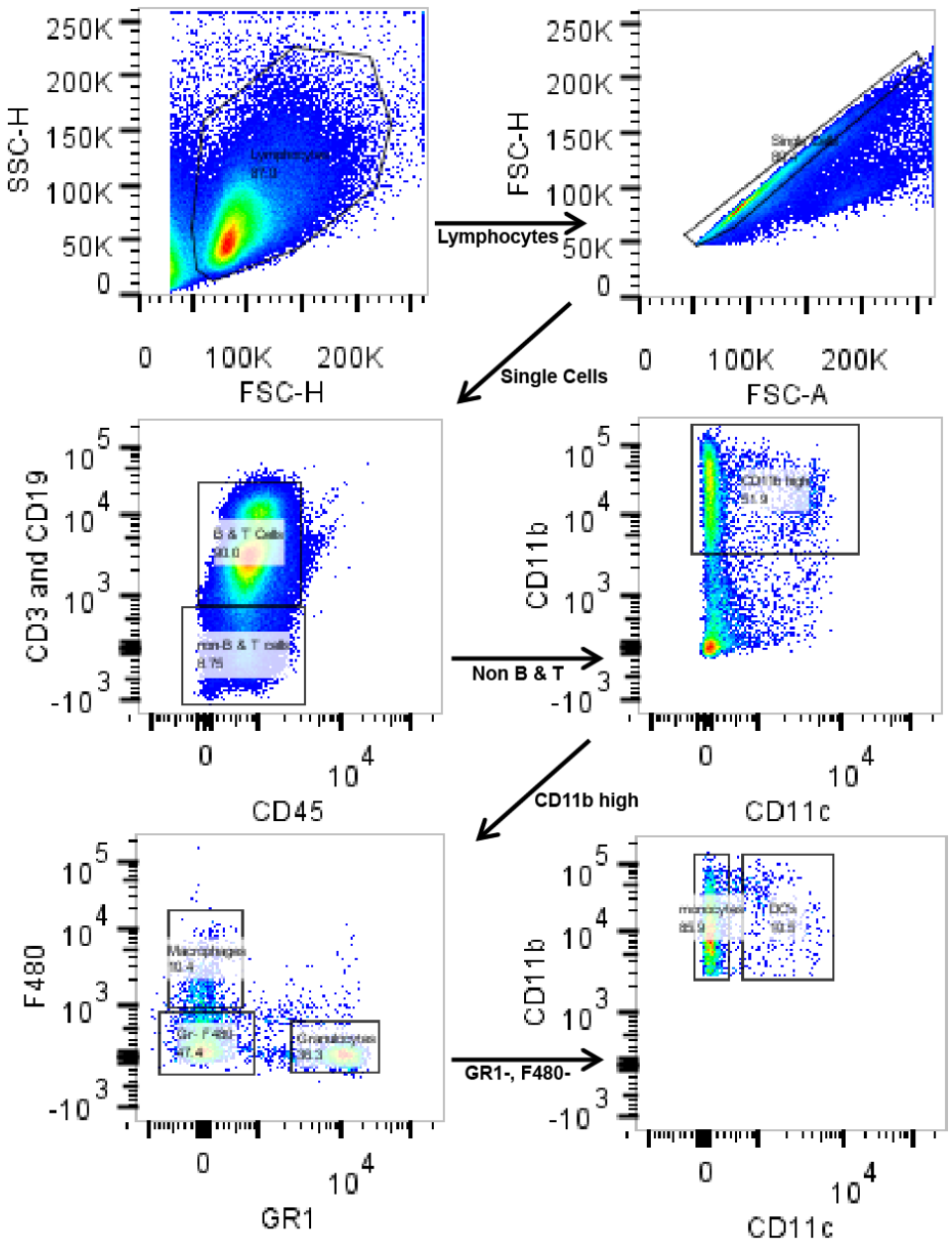

Figure 10. Representative gating scheme from BALB/c mouse spleen. Single lymphocytes were gated by side scatter vs. forward scatter. Single cells were divided into B & T cells VS. non B & T cells by expression of CD3 and CD19. For Non B & T cells those expressing high CD11b were selected for further analysis. CD11b high were plotted for F480 and GR1, GR1 high F480- were categorized as granulocytes, F480high GR1- were categorized as macrophages. GRI- F480- cells were further divided into monocytes (CD11c low), and DC's (CD11c high).

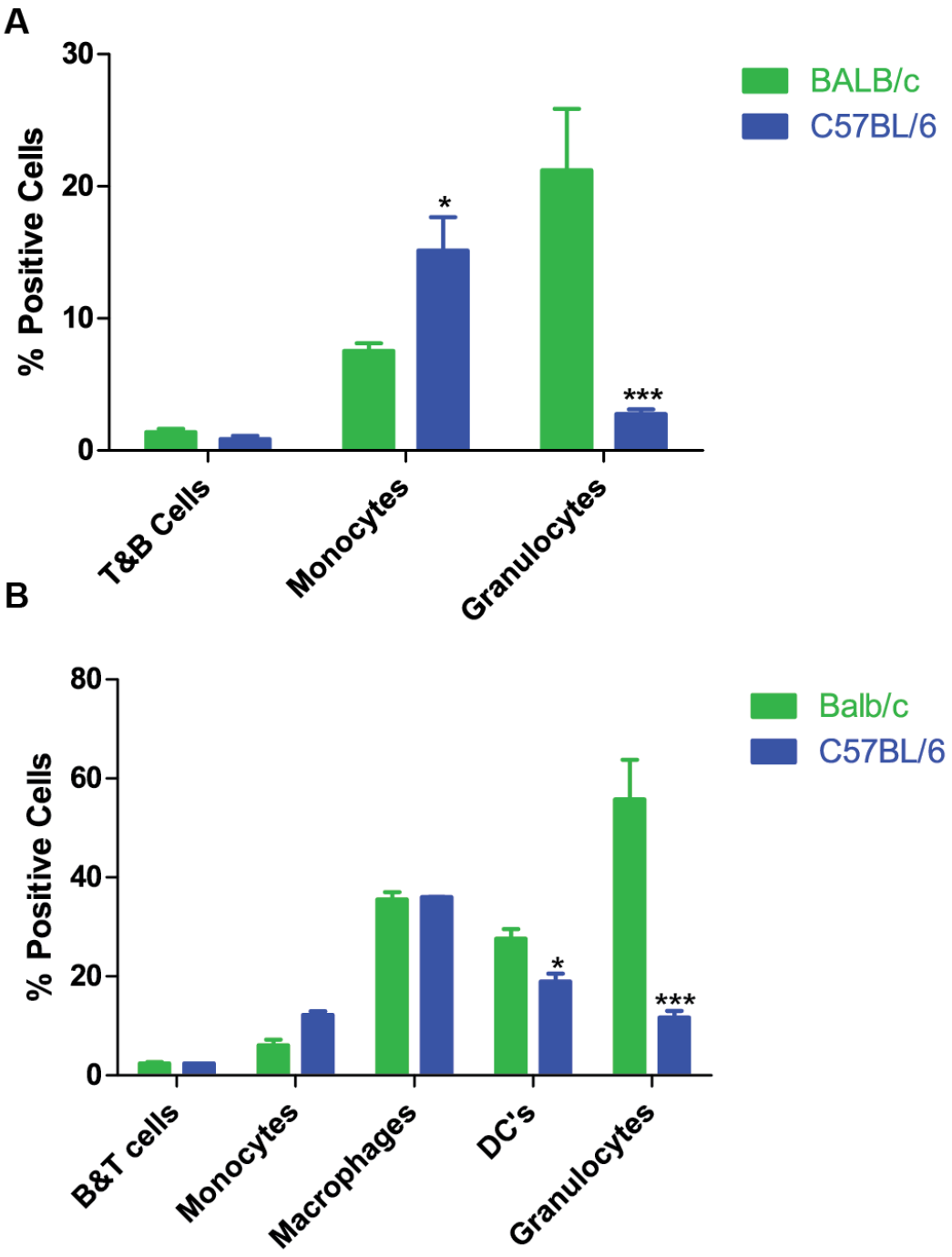

Figure 11: Flow cytometry of peripheral blood leukocytes and splenocytes shows dramatically higher uptake of particles by granulocytes in BALB/c mice.

(A) Flow cytometry of PBL's shows significantly higher uptake of particles by granulocytes in BALB/c mice ($p<0.002$, t-test), and significantly higher uptake by monocytes in C57BL/6 mice ($p<0.05$, t-test) (N=4).

(B) Flow cytometry of splenocytes shows significantly higher uptake of particles by DC's ($P < .05$, t test) and granulocytes ($p<0.003$, t-test) in BALB/c mice while monocytes take up significantly more particles in C57BL/6 mice ($p<0.05$, t-test) (N=4).

To address this idea directly, we depleted granulocytes from both strains by administering anti-Ly6-G antibodies, which has previously been shown to selectively deplete granulocytes in vivo *(Arnold et al., 2010).* Flow analysis confirmed that after antibody depletion, granulocyte numbers were reduced to below detection in both strains (Fig. 12). IVM was performed on both strains after granulocyte depletion to determine the effect on particle blood exposure. After granulocyte depletion, BALB/c mice showed equivalent peak fluorescence intensity compared to C57BL/6 mice (Fig. 13A), and a significant increase in particle blood exposure compared to untreated BALB/c mice (Fig. 13B). Conversely, C57BL/6 mice after granulocyte depletion showed no significant increase in peak fluorescence or particle blood exposure when compared to untreated C57BL/6 mice (Fig. 13B). These data indicate that some of the lower particle blood exposure (i.e., faster clearance) and lower peak particle concentration in BALB/c mice during the early passage through circulation is due to particle uptake by granulocytes in the blood.

To determine the fate of particles in the blood and spleen in the absence of granulocytes, we assessed particle uptake by immune populations in granulocyte-depleted mice using flow cytometry. Particle uptake by B and T-lymphocytes of blood and spleen were unaffected (Fig. 13C,D); however,

increased particle uptake by blood monocytes was observed in granulocyte depleted BALB/c mice, but not in C57BL/6 mice (Fig. 13C). In the spleen, granulocyte depletion did not affect monocyte uptake, but did increase macrophage uptake, with a greater increase in the BALB/c mice (Fig. 13D). Together, these data indicate that granulocytes account for some of the increased clearance seen in the BALB/c mice, but that in the absence of these cells, BALB/c mice still clear nanoparticles faster than C57BL/6 mice.

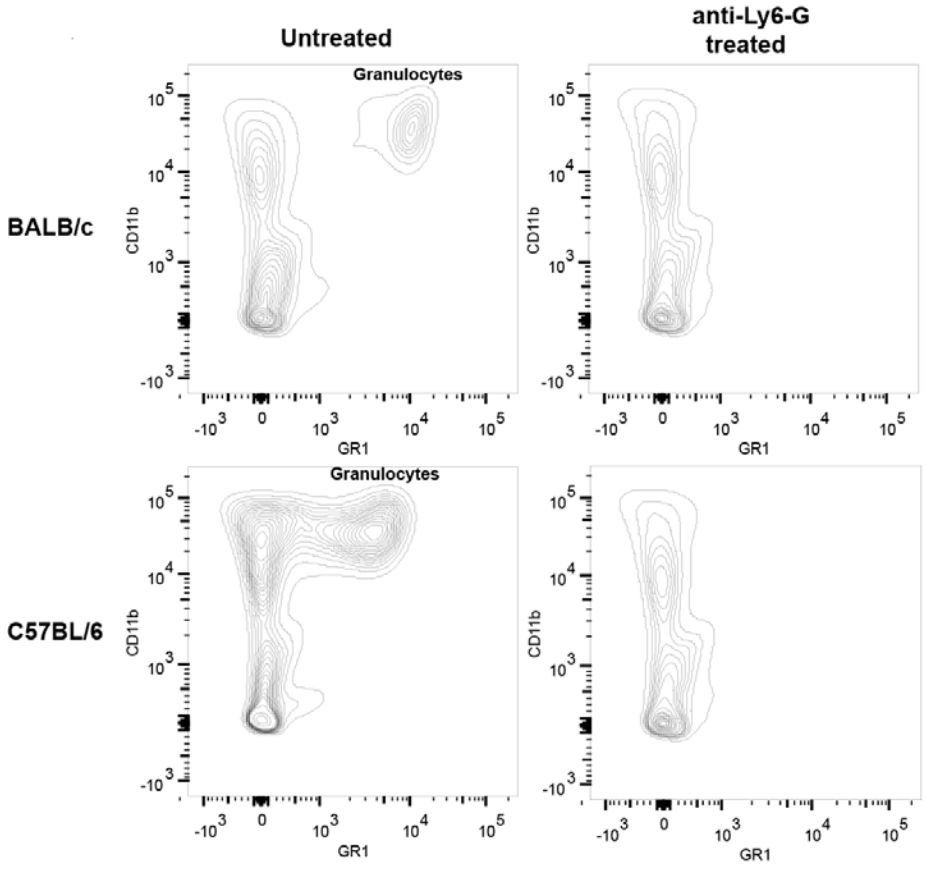

Figure 12: Depletion of granulocytes from mice using rat anti-mouse GR-1 antibodies.

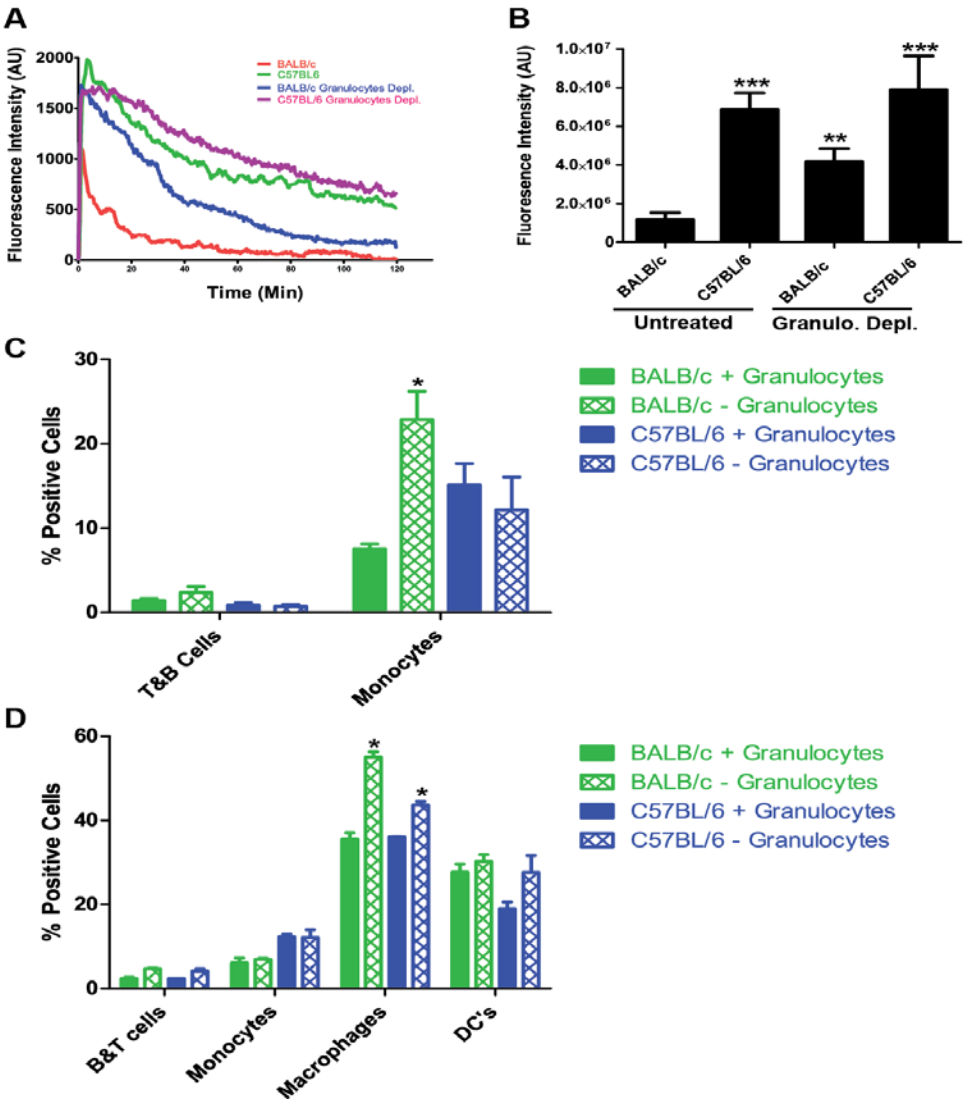

Figure 13: Depletion of granulocytes significantly increases particle exposure to blood in BALB/c mice but not C57BL/6 mice.

(A) Plots of fluorescence intensity versus time for four BALB/c and C57BL/6 mice with and without monocyte depletion (N=4 mice per condition).

(B) Plots of area under the curve show a significant increase in particle exposure to blood in BALB/c mice ($p<0.01$, One-way ANOVA, Dunnett post-test) but not C57BL/6 mice (N=4 mice per condition).

(C) Flow cytometry analysis of changes in PBL particle distribution in BALB/c and C57BL/6 mice following granulocyte depletion. BALB/c monocytes take up significantly more particles after granulocyte depletion ($p<0.05$, t-test) (N=3 mice for granulocyte depleted conditions and N=4 mice for controls).

(D) Flow cytometry analysis of splenocytes after granulocyte depletion in BALB/c and C57BL/6 mice. Macrophages in spleen take up significantly more particles after granulocyte depletion in both strains ($p<0.05$, t test) (N=3 mice for granulocyte depleted conditions and N=4 mice for controls).

Differential clearance of particles in Th1 vs. Th2 strains is dependent on particle type.

As a wide variety of nanoformulations are being investigated for potential clinical use and often demonstrate very different properties in vivo, we tested whether the differential clearance observed in various mouse strains is specific to the PRINT particles (300 nm, PEG hydrogel). We tested the blood exposure of quantum dots (Qdots) in BALB/c and C57BL/6 mice. The quantum dots were polymer coated with a carboxylated polymer that prevents aggregation in aqueous environments. The Qdots tested are a different class of nanoparticle (inorganic nanocrystal VS hydrogel) with a different surface (proprietary carboxilated polymer vs. PEG), a different shape (sphere vs. cylinder) and an order of magnitude smaller (avg size 30nm Qdots vs. 300nm cylindrical PRINT hydrogels (Fig. 4A-C). Upon IV injection, the Qdots were more rapidly removed from blood by both BALB/c and C57BL/6 mice than PRINT particles. However, the Th1 vs. Th2 biased strain clearance difference was still present (Fig. 14A, B), including a lower peak fluorescence intensity with Qdots, suggesting that a large number of Qdots are cleared in the periphery of BALB/c mice. To test if microparticles display the same effect in Th1 vs. Th2 strains, we utilized low elastic modulus PRINT microparticles (6 μm disks made of the same PEG hydrogel materials as 300nm cylindrical PRINT hydrogels) that were previously demonstrated to have long circulation times and are not cleared by mechanical

filtration in the lungs (Merkel et al., 2011). Interestingly, BALB/c and C57BL/6 mice demonstrated the same microparticle exposure to blood (Fig 14C, D), suggesting that rapid removal of nanoparticles in Th2 prone strains is not observed with larger particles requiring phagocytic clearance.

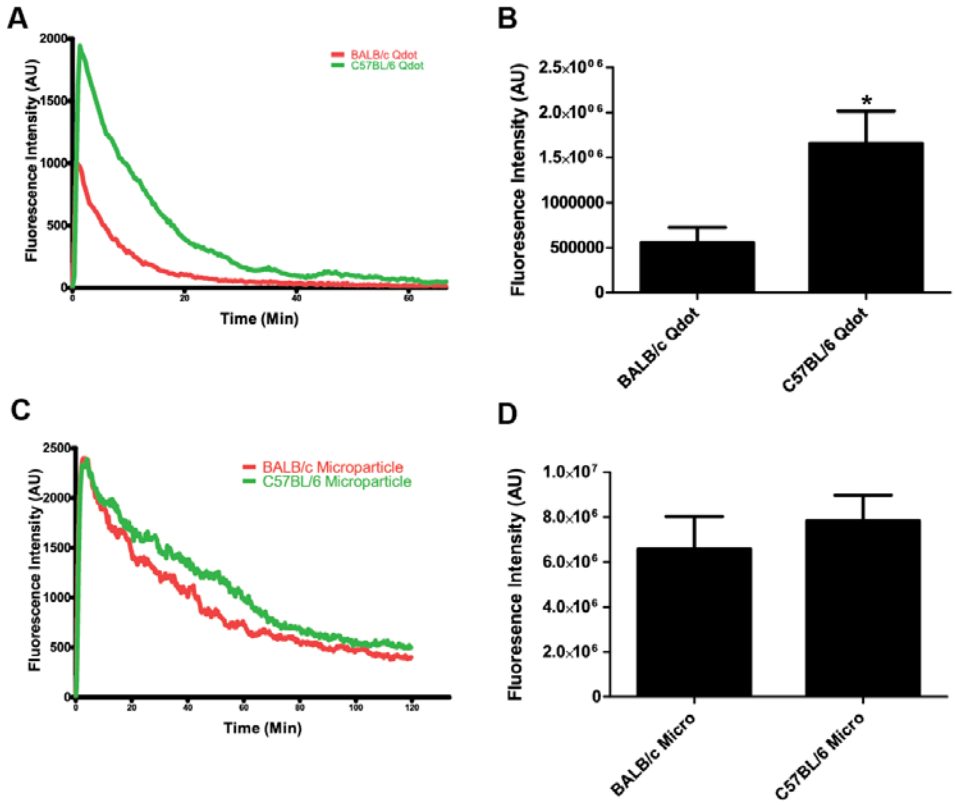

Figure 14: Depletion of granulocytes significantly increases particle exposure to blood in BALB/c mice but not C57BL/6 mice.

(A) Plots of fluorescence intensity versus time for quantum dots in blood of BALB/c and C57BL/6 mice show a similar trend to what was observed with 300 nm PRINT hydrogel particles (N=4).

(B) Area under the curve shows a significant ($p<0.05$, t-test) increase in blood fluorescence from quantum dots in C57BL/6 mice VS BALB/c mice.

(C) Plot of fluorescence intensity in blood versus time for BALB/c and C57BL/6 mice show similar clearance rates for microparticles.

(D) Area under the curve analysis of blood fluorescence intensity from both strains shows no significant difference.

Murine bone marrow derived macrophages and primary human peripheral blood monocyte-derived macrophages take up more particles with M2 polarization.

We examined if differential clearance by Th1 and Th2 prone strains can be reproduced in vitro by culturing primary bone marrow derived macrophages (BMM) from both strains and testing particle uptake by BMMs. We chose to use BMMs as opposed to granulocytes due to the fact that BMMs can be maintained in culture for longer time periods, thus allowing treatment with Th1 and Th2 cytokine mixtures to polarize these macrophages towards M1 or M2 phenotypes, respectively. We imaged the accumulation of particles inside the macrophages and quantified the integrated fluorescence intensity of particles per cell. We also processed cells for analysis by flow cytometry. Consistent with our in vivo observations, untreated BALB/c macrophages take up significantly more particles than untreated C57BL/6 macrophages in vitro as assayed by both confocal microscopy and flow cytometry (Fig. 15A, B). BMMs from both strains were also directed towards M1 or M2 polarization by specific mixtures of cytokines and immune stimulators (see Materials and Methods). M1 polarization of C57BL/6 macrophages had no effect on particle uptake, while differentiation into the M2 phenotype resulted in an increase in particle uptake (Fig. 15A, B). Conversely, M1 polarization of BALB/c macrophages reduced particle uptake to the same

level as C57BL/6 macrophages, while M2 polarization showed no significant difference compared to BALB/c control (Fig. 15A, B).

As significant differences are known to exist between mouse and human macrophages (Mestas and Hughes, 2004),we repeated particle uptake experiments with human monocyte-derived macrophages from two healthy human volunteers. Volunteer A's macrophages showed high uptake of particles with no stimulation, a significant reduction in uptake with M1 polarization, and no difference with M2 polarization (Fig. 15C). Volunteer B's macrophages showed intermediate uptake of particles with no stimulation, a significant decrease in uptake with M1 polarization, and a significant increase in uptake with M2 polarization (Fig. 15D). These results confirm that immune polarization fundamentally impacts cellular interactions with nanoparticles in human cells.

One significant difference between M1 and M2 macrophages is that M2 macrophages are known to express higher levels of many different scavenger and lectin receptors than M1 macrophages. Flow cytometric analysis of revealed increased MMR (macrophage manose receptor) expression on the surface of BALB/c macrophages (BMMs) compared to C57BL/6 macrophages (Fig. 15E), which is consistent with previously published transcriptional profiling data (35,38). To test whether the differential uptake of particles by BALB/c and C57BL/6 macrophages is MMR-dependent, we treated with BMMs with the competitive MMR inhibitor mannan prior to addition of particles. Mannan reduced particle

uptake in BALB/c macrophages to the same level as C57BL/6 macrophages while showing no effect on C57BL/6 macrophages, suggesting that the increased level of MMR present on M2 macrophages in BALB/c mice may contribute to differences in particle uptake in vitro (Fig. 15F) and (Fig 16).

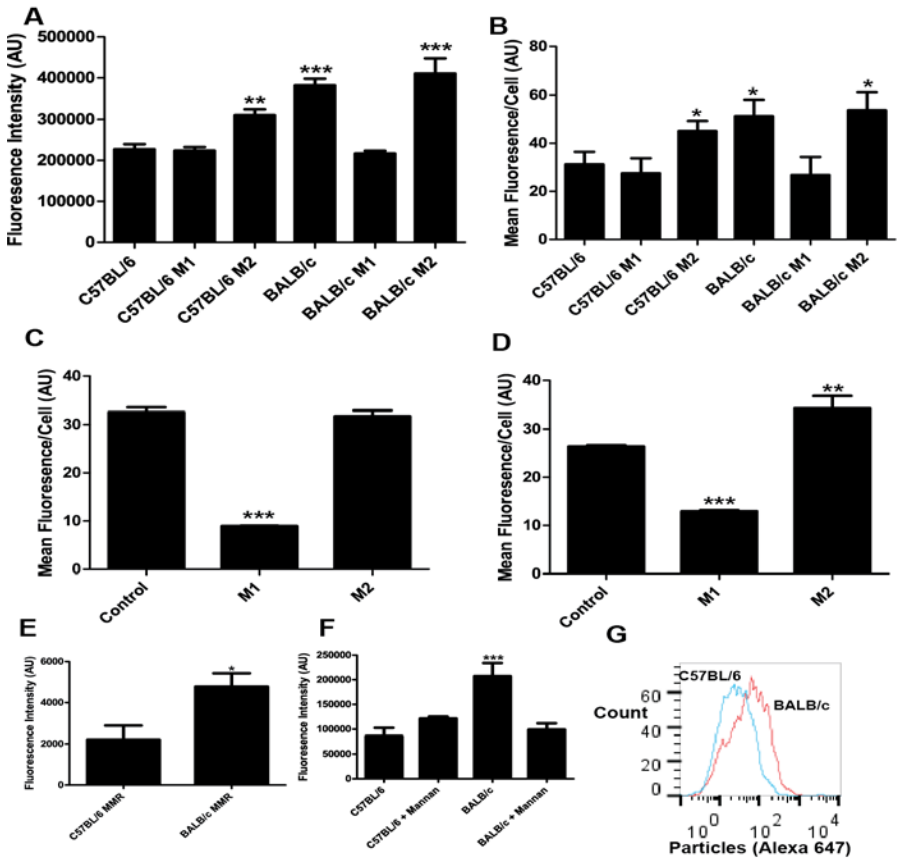

Figure 15: M2 polarized macrophages take up more particles than M1 macrophages in mice and humans.

(A) Average integrated fluorescence per cell showed a significant ($p<0.0001$, One-way ANOVA Dunnett's post-test) increase in particle uptake by BALB/c untreated, BALB/c Th2-treated, and C57BL/6 Th2-treated VS C57BL/6 untreated cells. C57BL/6 M1-treated and BALB/c M1-treated showed no significant difference vs. C57BL/6 untreated Cells (N=4).

(B) Flow cytometry analysis of uptake showed a significant ($P<0.05$, One-way ANOVA Dunnett's post-test) increase in uptake by BALB/c untreated, BALB/c Th2-treated, and C57BL/6 Th2-treated VS C57BL/6 untreated cells. C57BL/6 M1-treated and BALB/c M1-treated showed no significant difference vs. C57BL/6 untreated cells (N=4).

(C) Flow cytometry analysis of uptake by human macrophages from volunteer A. M1 macrophages took up significantly less particles than control or M2 macrophages ($P<0.0001$, One-way ANOVA Dunnett's post-test) (N=4).

(D) Flow cytometry analysis of uptake by human macrophages from volunteer B. M1 macrophages took up significantly less than control macrophages ($P<0.0001$, One-way ANOVA Dunnett's post-test). M2 macrophages took up significantly more than control macrophages ($P<0.001$, One-way ANOVA Dunnett's post-test) (N=4).

(E) Flow cytometry analysis of surface MMR expression on Balb/c and C57BL/6 mice. Balb/c mice showed significantly higher surface expression of MMR ($P<0.05$, t-test) (N=4).

(F) Microscopy analysis of uptake by BMMs after mannan blocking. Addition of Mannan reduced uptake by Balb/c macrophages to the same levels as C57BL/6 controls ($P<0.0001$, One-way ANOVA Dunnett's post-test)(N=4).

(G) Representative flow cytometry histogram of particle uptake by BALB/c and C57BL/6 BMM's.

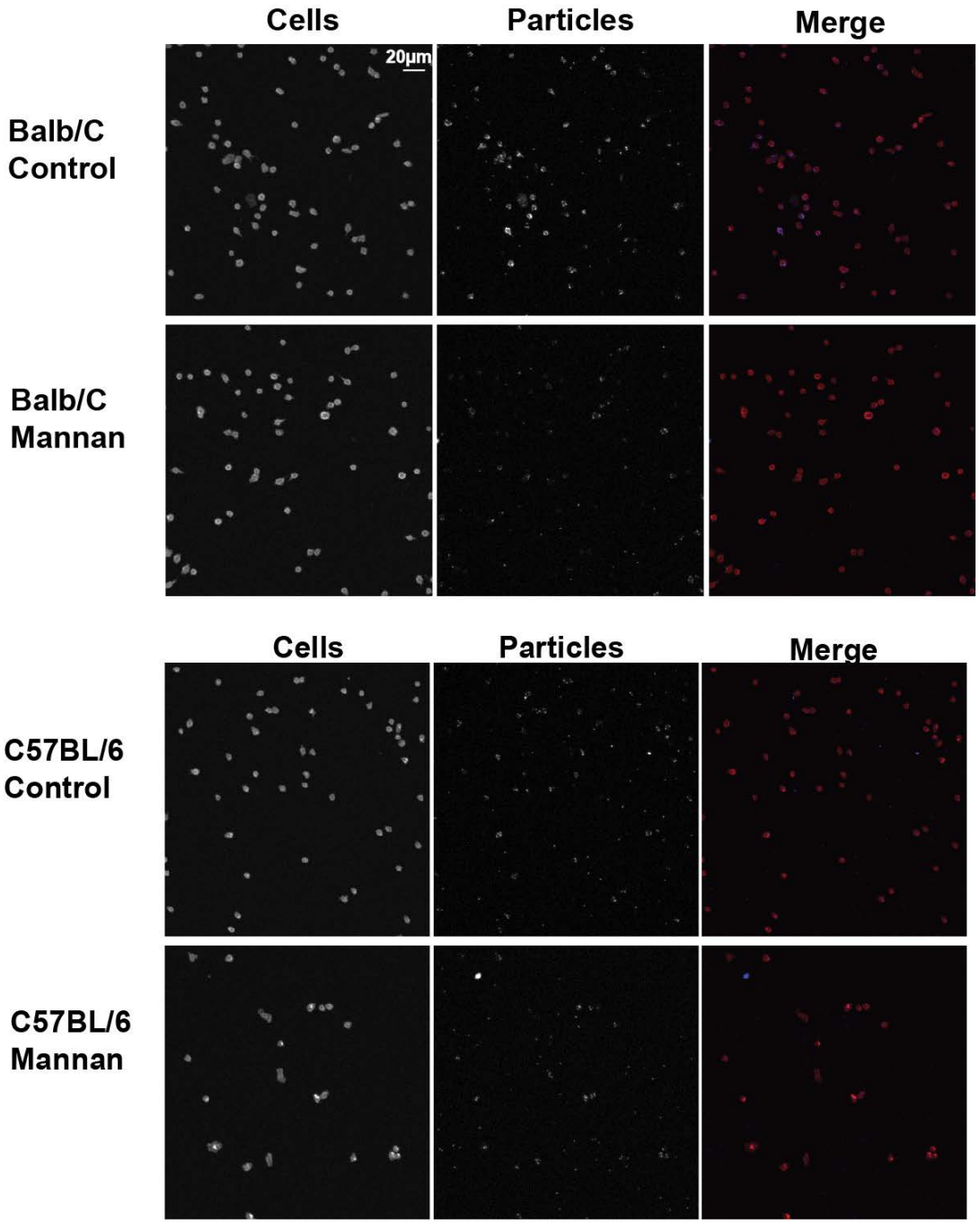

Figure 16: Confocal microscopy of Balb/c and C57BL/6 BMMs with and without mannan treatment.

DISCUSSION

In this study, we have identified a striking difference in nanoparticle clearance in different strains of mice that arises due to differences in global immune status differences. Th1-prone strains such as C57BL/6 clear particles more slowly and have a higher blood exposure compared to the Th2-prone BALB/c strain that demonstrated rapid particle clearance. Both monocytes/macrophages and granulocytes in the peripheral vasculature and spleen are responsible for clearance differences between the strains. Interestingly, the differences in clearance were recapitulated in vitro using mouse and human macrophages treated with either Th1 or Th2 chemokine/cytokine mixtures. This effect may be due, in part, to differences in surface expression of scavenger receptors such as the macrophage mannose receptor (MMR).

In most studies nanoparticle PK is determined by blood draws at specific time points post injection, combined with appropriate assays for determining the particle concentration in blood (Chu et al., 2012; Kulkarni and Feng, 2013). This method has the advantage of directly measuring the particle itself rather than a reporter probe and provides absolute particle concentration in the blood. However, this approach requires large numbers of animals and particles to yield useful data. Most experiments of this type require four animals or more per time point, and at least five time points plus a control for a minimum of 24 animals

needed for each condition tested. This makes blood draw assays an unattractive option for screening multiple types of animals and/or particle types due to the high time and resource investment required. In addition, blood draw PK tends to give very limited temporal resolution, usually seven or fewer points per 24hr experiment (Caron et al., 2012).

Intravital microscopy (IVM) has a number of advantages for measuring nanoparticle clearance. With IVM, the relative amount of particles in the bloodstream is measured with a wide dynamic range allowing for measurements spanning pre-injection to peak particle concentration through clearance in a single animal. Fluorescent probes can be directly incorporated into hydrogel nanoparticles during synthesis, therefore eliminating the need for extensive post-fabrication modifications. In addition, this technique is very fast, allowing for real time or near real time measurement of relative particle concentrations. Finally, IVM can be multiplexed with different fluorescent dyes coupled to different particle types or formulations to measure differential clearance in the same animal. However, IVM is limited by the fact that only relative numbers are readily available from this type of experiment, the particle must be fluorescent, and it is difficult to run experiments longer than 3hrs due to the stress on the animal from extended anesthesia.

The nanoparticle research field operates under the implicit assumption that nanoparticles will circulate in similar ways in all strains of mice. We are

unaware of any previous study that has directly compared the effect of mouse strain on nanoparticle circulation times. Our results indicate mouse strain background is a critical factor for nanoparticle clearance and is likely important for the interpretation of all results of nanomedicine studies. In fact, the changes in circulation times observed between Th1 and Th2 prone mouse strains is equivalent to the changes that can be produced by heavily PEGylating particle surfaces (Perry et al., 2012). This demonstrates that changes in the immune status of patients and experimental animals may affect nanoparticle PK to at least the same degree as the material properties of particles. However, far less work has been done studying the effects of biology on nanoparticle PK than the effects of material properties on nanoparticle PK. It is perhaps not surprising that we see different results in different mouse strains for clearance, as mouse strain background has significant impact on biological processes ranging from immune function (Kastrukoff et al., 2012), pain sensation (Mogil et al., 1999) and cancer (Mesquita et al., 2012). Outbred, wild mice show a large degree of heterogeneity in many measures of immune function, while inbred lab strains of mice show very little intrastrain variation (Abolins et al., 2011). In the future, it would be beneficial for researchers in the nanoparticle field to begin explicitly considering mouse strain immunology when designing experiments and interpreting data.

Based on our results, global immune system regulation has a significant role in nanoparticle clearance. One main global immunological difference is Th1

vs. Th2 status. Numerous studies have established that Th1 and Th2 cytokines can induce macrophage differentiation into the corresponding M1 and M2 phenotypes (Gordon and Martinez, 2010). The result that Th1 prone mice (eg. C57BL/6) clear nanoparticles slower is somewhat surprising as M1 macrophages are thought to be more inflammatory, involved in the destruction of pathogens, and have been shown to be more phagocytic towards *S. aureus* (Krysko et al., 2011). The M2 macrophages prevalent in the fast clearing Th2 stains are generally thought to be anti-inflammatory, with involvement in wound healing and potentially less phagocytic (Gordon and Martinez, 2010). However, M2 macrophages are thought to have higher levels of endocytosis and may thereby take up small particles rapidly. In addition, M2 macrophages are known to express higher levels of scavenger and lectin receptors that could be responsible for the increased clearance (Martinez et al., 2006). Our data on the elevated surface expression of MMR on M2 macrophages and the reduced nanoparticle uptake upon mannan treatment support this notion.

While the addition of mannan blocks the enhanced uptake of PEG hydrogel particles in M2 macrophages in vitro, a baseline uptake of particles still occurs with treatment. Indeed, clearance in vivo likely involves multiple receptors and mechanisms. Determining which receptors are responsible for nanoparticle clearance is an important next step. Unfortunately, the obvious genetic approach of using knockout mice (KO) in candidate clearance receptors is severely complicated by the fact that most of these KO's exist only in the

C57BL/6 strain. Since treatment of the slow-clearing C57BL/6 mice with clodronate liposomes (removing all MPS cells) did not show a statistically significant increase in nanoparticle circulation times in a 2hr window, it is unlikely that the genetic loss of any single candidate clearance receptor would produce a measurable decrease in nanoparticle clearance. In the future, it will be essential to backcross these KO's into the BALB/c background where these experiments are likely to produce more informative results.

It is also worth considering the role of granulocytes (primarily neutrophils) in nanoparticle clearance. Although this cell type is rarely discussed as an MPS cell (Rabinovitch, 1995; Silva and Correia-Neves, 2012), our data clearly indicates that granulocytes play a significant role in the differential nanoparticle clearance observed between mouse strains. Previous reports indicate that BALB/c mice have greater numbers of circulating granulocytes than C57BL/6 mice (Petkova et al., 2008). Our data indicate that mere differences in granulocyte numbers are unlikely to account for the clearance differences between strains, as a smaller percentage of C57BL/6 granulocytes take up particles than BALB/c granulocytes. Since neutrophils constitute a large fraction of circulating white blood cells in humans (Bishton and Chopra, 2004) and neutropenia is a common side effect of clinical treatments such as chemotherapy, it will be important to further explore the role of neutrophils in nanoparticle clearance in future studies.

Similar to our results with mice, the pharmacokinetics of nanoparticles is highly variable in human patients (Caron et al., 2012). Previous studies demonstrated that monocyte function, as assayed by phagocytic capacity and oxidative burst, can be used to predict the clearance of liposomal Doxil (Caron et al., 2012). Since both the phagocytic capacity and oxidative burst are partially controlled by the patient's global immune status (Mills et al., 2000), it is likely that the Th1/Th2 balance is an important factor in human nanoparticle clearance as well. This is supported by our results with human macrophages that showed a significant decrease in particle uptake from both volunteers' macrophages following M1 polarization, and one volunteer's macrophages showing an increase in uptake with M2 polarization. Future studies are needed to explore the role of previous immune priming events such as infections or allergies on nanoparticle clearance. Our data suggest that a more comprehensive understanding of how global immune regulation affects nanoparticle clearance will be important both for nanoparticle studies in animals and eventual clinical use.

CHAPTER FOUR: FUTURE DIRECTIONS

The nature of the interactions between nanoparticles and the immune system still requires significant study to be fully understood, appreciated and manipulated. The work presented here suggests promising avenues to be pursued and provides several valuable tools to use in future work. In this chapter I will address some, although certainly not all, possible future work that can derived from the foundation of this body of work.

Genetic Factors Controlling Th1/Th2 Polarization and Nanoparticle Clearance

This work has shown a clear correlation between Th1 and Th2 immunity and particle clearance. However it also suggests that the relationship may be more complicated than a simple interpretation of Th2 cytokines produce M2 macrophages which clear particles more rapidly than M1 macrophages. Three results in particular suggest a more complex explanation is needed to fully explain the above results. First, non-diseased mice have cytokine levels that are extremely low or below detection.This means that resting macrophages in these mice should be relatively non-polarized towards either M1/M2 activation states. Secondly, isolated primary macrophages from BALB/c and C57BL/6 mice show a difference in particle uptake with no additional cytokine treatments

after identical treatment with L-media and serum which contain the same base line of cytokines. This suggests that there is some type of basal genetic difference between BALB/c and C57BL/6 macrophages that, while correlated with Th1/Th2 prone states, exists independent of cytokine stimulation. Finally, the dramatic difference observed in neutrophil activity towards particles in BALB/c vs C57BL/6 suggests that differences between Th1 and Th2 cytokine activity is not the entire story, as short lived neutrophils in healthy mice will have seen very little in the way of cytokines during their life cycle. These three data points suggest that there is some upstream genetic difference causing the Th1/Th2 polarization, the differences in particle uptake by unstimulated macrophages, and the differences in particle uptake by neutrophils. Determining what this driving genetic difference is could both reveal important aspects of how the immune system interacts with nanoparticles, as well as important genetic regulation of Th1/Th2 immunity and its relationship to innate immunity.

A likely way to address this is using the collaborative cross mice (Churchill et al., 2004). The collaborative cross was performed by taking a number of lab mouse strains and wild caught mice from around the world and breeding them together for several generations before deriving a large number of new inbreed strains, with each of these new strains being exhaustively genetically profiled at the sequence and transcriptome level. By combining this model set with the intravital microscopy PK assay described in this work we would have an excellent chance at determining what alleles are responsible for

slow and fast nanoparticle clearance by determining which collaborative cross strains clear faster or slower, and grouping these datasets. This can then be followed by in depth genome and transcriptome analysis to determine which alleles are consistently altered in fast and slow clearing mice. Determining which genetic pathways are consistently changed in fast vs slow clearing mice may allow us to both predict candidate receptors on macrophages and neutrophils which could be blocked to extend clearance, or pathways which could be drugged to extend particle circulation.

Determination of Gene Products Controlled by Th1/Th2 Cytokines That Clear Nanoparticles

Ultimately the most likely way to extend the circulation time of nanoparticles *in vivo* is to block the receptors on macrophages that bind and clear particles. This is preferential to drug treatments that inactivate phagocytes as it will have fewer off-target effects and leave patients less immune suppressed. However in order to generate function blocking antibodies or FAB fragments against the relevant phagocytic receptors we must first positively identify which receptors mediate nanoparticle clearance. We anticipate that this can be accomplished in mice using two approaches. First we will need to isolate some combination of macrophages, neutrophils and monocytes from BALB/c, DBA2, C57BL/5 and B10D2 mice. From these cells RNA can be extracted and analyzed by RNA deep sequencing technology to generate an accurate transcriptome of each of these cell populations from each mouse type. The

same can be done on BALB/c and C57BL/6 BMM's either untreated or treated with cytokines. These samples can then be grouped into two distinct populations of cells that take up large numbers of particles and cells that do not. We can then analyze the transcriptomes of these cells and determine which specific phagocytic receptors have been up regulated in the fast clearing cells versus the slow clearing cells. Any receptors that are consistently up in fast clearing cells can then be confirmed by quantitative PCR analysis and Western to ensure that they represent genuine targets.

After determining what receptors are consistently expressed at higher levels on phagocytes that clear particles rapidly we can purchase mice that have had the receptors knocked out in most cases. Unfortunately these receptors are typically knocked out in C57BL/6 mice, which means to use our IVMPK assay we must back cross them onto a BALB/c background. This will take approximately two years two accomplish, and so should only be performed for receptors that have been implicated by the genetic approaches above. But once the backcross is complete we can analyze particle circulation times by IVMPK to determine the relative impact of each receptor type on particle clearance.

Finally for any receptors that have been confirmed to be relevant for clearing nanoparticles in knockout mice, we can either purchase or generate function blocking antibodies or FAB fragments against them. These can then be administered prior to nanoparticle injection to block particle uptake and confirm the functionality of inhibiting the implicated receptors. Any receptors that show

positive effects from being blocked can be considered for the generation of anti human function blocking antibodies for evaluation in the clinic for extending the circulation time of nanoparticles in patients.

Further Elucidation of Th1/Th2 Effects on Nanoparticle Clearance

As discussed above it is unlikely that Th1/Th2 immune status is the sole driver in the differential clearance we observed in this study. However the *in vitro* data clearly demonstrates that Th1/Th2 cytokines can affect the clearance of nanoparticles by primary human and mouse macrophages. It is therefore worth further elucidating this response *in vivo* using several common immunological assays.

First, our data clearly shows that BMM's from BALB/c and C57BL/6 mice have differential particle uptake phenotypes independent of cytokines and T cell signals. However it is unclear if this is due to activity of T cell cytokines earlier in the development of these cells in mice, or due to inherent genetic differences in the macrophages themselves. To test we can first examine the clearance of nanoparticles in several mouse models with modified T cell characteristics. Nu/Nu mice that lack proper thymuses and therefore lack T cells can be purchased in both the BALB/c and C57BL/6 background allowing us to determine if clearance of particles *in vivo* is altered by the loss of T cells in these mice. In addition Rag-/- BALB/c and C57BL/6 mice are available that have proper thymuses, but do not result in adult T cells *in vivo*, these mice can be compared to wild type and Nu/Nu mice to determine if mature T cells,

immature T cells, or no T cells are required for the observed differences in nanoparticle circulation. Additionally in all of these models Th1 or Th2 T cells from background matched wild type mice can be transferred into the T cell deficient mice to see if this can rescue/change observed particle uptake phenotypes. These experiments should allow us to determine the relative impact on T cell signaling versus genetic differences in other cell types in the mouse on particle uptake.

Second while BALB/c and C57BL/6 mice are known to be Th1/Th2 prone these are not true Th1/Th2 immunity models as cytokine levels remain low. It would therefore be better to test the effect of Th1 and Th2 immunity on particle clearance in disease models that are well characterized to generate these responses. To do this we would first determine the base circulation profile in the C3H/HeN mouse strain which is capable of having either a Th1 or Th2 immune response. After determining the basal clearance of particles we can infect another group of HEN mice with helminth parasitic worms which are well characterized to generate Th2 immune responses, and or induce experimental asthma which is also know to involve Th2 responses. A second group can be infected with gram positive bacteria and or yeast infection to induce Th1 immune responses. We can then determine the effect of these treatments on clearance of particles both during and after the immune response to see if particle clearance is affected as expected in both the short term and the long term by Th1/Th2 immunity.

Finally, to examine the effect of stromal cells versus immune cells on particle clearance BALB/c and C57BL/6 mice can be irradiated to kill all bone marrow. After irradiation, bone marrow transplantation can be performed with strain matched or reversed bone marrow. This will be followed up with multiple rounds of clodrinate injections to remove tissue macrophages from the original bone marrow. If BALB/c mice with BALB/c bone marrow and C57BL/6 mice with BALB/c bone marrow clear particles rapidly while C57BL/6 mice with C57BL/6 bone marrow and BALB/c mice with C57BL/6 bone marrow clear particles slowly this indicates that differences in the immune system are responsible for the observed differences in particle uptake. If, however, the opposite were observed, it would suggest that signaling contributions from the stromal cells early in phagocyte differentiation are instead responsible for establishing the observed differences in particle clearance.

Combining these three experiments together should result in a much more complete understanding of the exact role of Th1/Th2 immunity on particle clearance.

Clinical Studies

In this work we demonstrated that with a limited sample (N=2) human primary blood monocyte derived macropahges behaved similarly to mouse macropahges in regards to particle uptake with M1/M2 polarization. However there was a substantial difference in the base line uptake of particles by

macrophages from the two volunteers. As the value of this work is ultimately to improve the efficacy of nanomedicine in human patients it will be important to expand on these preliminary experiments with human cells in three ways. First and most simply, we need to test a much larger number of human samples. This should be done by drawing blood from 20-30 individuals; part of it should be used to derive macrophages as done in this study and test baseline uptake of particles and the effect of Th1/Th2 cytokine treatment on particle uptake. Secondly, we will also dose sample of whole blood from each volunteer with particles and then perform flow cytometry on it. This will allow us to determine if we see significant differences in the capacity of neutrophils from the different volunteers to uptake particles the same way we see differences with different mouse strains. Finally we will run ELISA assays for Th1 and Th2 cytokines on the plasma from the blood samples and look for correlations between uptake by primary macrophages and by neutrophils in whole blood samples to levels of Th1 and Th2 cytokines from volunteers. After establishing baseline readings from healthy human volunteers we can get blood samples from clinical patients who are experiencing pathological conditions known to elicit Th1, Th2 or Th17 immune responses. Examples can include asthma or severe allergies for Th2, bacterial or yeast infections for Th1, or severe viral infections or autoimmune conditions for Th17. These samples can then be analyzed in the same way as the healthy volunteer's samples to determine if the anticipated changes in phagocyte behavior from the mouse studies are seen in human samples. Finally, there are large numbers of ongoing clinical trials for a diverse range of

nanoparticles as well as patients being treated with the approved nanoformulation Doxil. We can acquire blood samples from these patients as well as detailed PK results from these patients in clinical studies. We can then analyze the blood from the patients for levels of Th1 and Th2 cytokines and phagocyte behavior and determine how this correlates to observed PK data in patients. We predict that we will be able to determine appropriate assays for cytokine levels to predict if patients being treated with nanoparticles are likely to clear particles quickly or slowly. In addition if we experience success with identifying important receptors in clearance and generating function blocking antibodies against them, then in the distant future we may be able to alter the PK of nanoformulations in patients with these reagents.

APPENDIX A:

MATERIALS AND METHODS:

Particle Materials and Methods:

Materials

Poly(ethylene glycol) diacrylate (M_n 700) ($PEG_{700}DA$), 2-aminoethyl methacrylate hydrochloride (AEM), diphenyl (2,4,6-trimethylbenzoyl)-phosphine oxide (TPO), and sucrose were purchased from Sigma-Aldrich. Thermo Scientific Dylight 650 maleimide, PTFE syringe filters (13 mm membrane, 0.22 µm pore size), and methanol were obtained from Fisher Scientific. Conventional filters (2 µm) were purchased from Agilent and polyvinyl alcohol (Mw 2000) (PVOH) was purchased from Acros Organics. PRINT molds (200 nm x 200 nm) were obtained from Liquidia Technologies. Tetraethylene glycol monoacrylate (HP_4A) was synthesized in-house.

PRINT Nanoparticle Fabrication

The pre-particle solution was prepared by dissolving 5 wt% of the various reactive monomers in methanol. The reactive monomers included: a cure-site monomer (an oligomeric PEG with a nominal molar mass of 700 g/mol terminally functionalized on both end groups with an acryloxy functionality), a hydrophilic monomer used to make up the majority of the particle composition (HP4A), a polymerizable fluorescent tag (Dylight 650 maleimide), and a photoinitiator. The pre-particle solution was comprised of 87.5 wt% HP_4A, 10 wt% $PEG_{700}DA$, 1.5 wt% Dylight 650, and 1 wt% TPO. Using a # 3 Mayer rod

(R.D. Specialties), a thin film of the pre-particles solution was drawn onto a roll of freshly corona treated PET using a custom-made roll-to-roll lab line (Liquidia Technologies) running at 12 ft/min. The solvent was evaporated from this delivery sheet by exposing the film to a hot air dam derived from heat guns. The delivery sheet was laminated (80 PSI, 12 ft/min) to the patterned side of the mold, followed by delamination at the nip. Particles were cured by passing the filled mold through a UV-LED (Phoseon, 395 nm, 30 PSI N_2, 12 ft/min). A plasdone harvesting sheet was hot laminated to the filled mold (140ºC, 80 PSI, 12 ft/min). Upon cooling to room temperature, particles were removed from the mold by splitting the harvesting sheet from the mold. Particles were then harvested by dissolving the plasdone in a bead of water (1 mL of water per 5 ft of harvesting sheet). The particle suspension was passed through a 2 µm filter (Agilent) to remove large particulates. To remove the excess plasdone, particles were centrifuged at ca. 21,000 x g for 15 min, the supernatant was removed and the particles were re-suspended in sterile water. This purification process was repeated 4 times.

Nanoparticle Characterization

Stock particle concentrations were determined by thermogravimetric analysis (TGA) using a TA Instruments Q5000 TGA. TGA analysis was conducted by pipetting 20 µL of the stock particle solution into a tared aluminum sample pan. Samples suspended in water were heated at 30°C/min to 130°C, followed by a 10 minute isotherm at 130°C. Samples were then cooled at 30°C/min to 30°C,

followed by a 2 minute isotherm at 30°C. TGA was also performed on a 20 µL aliquot of supernatant from a centrifuged sample of the stock nanoparticle suspension to account for the mass of any stabilizer remaining in each sample. The supernatant concentration was subtracted from the concentration of stock particle suspension to determine the actual particle concentration. Particles were visualized by scanning electron microscopy (SEM) using a Hitachi S-4700 SEM. Prior to imaging, SEM samples where coated with 1.5 nm of gold-palladium alloy using a Cressington 108 auto sputter coater. Particle size and zeta potential were measured by dynamic light scattering (DLS) on a Zetasizer Nano ZS (Malvern Instruments, Ltd.).

Microparticle Fabrication

PRINT molds made of perfluoropolyether were received from Liquidia Technologies (NC, USA). The RBC mimics--starting from a pre-polymer composition of 87% 2-Hydroxyethyl acrylate (sigma), 10% 2-Carboxyethyl acrylate (sigma), 1% Poly(ethylyeny glycol) diacrylate (MW=4,000) (PolySciences), and 1% DyLight 650 malemide (ThermoScientific)--were made using a mold that had discoid feature with 2 µm diameters and heights of 0.6 µm. Briefly, the pre-polymer mixture was spread onto a piece of the mold (0.5×0.5 ft.) that was chilled to 2-5°C on a custom-built laminator platform to avoid monomer evaporation prior to photocuring. A poly(ethylene terepthalate) (PET) sheet was laminated to the top of the mold and pre-polymer solution, wetting the total mold area. The sheet was peeled away at the nip point of the

laminator, leaving the wells of the mold filled while wicking away excess solution. The filled mold was immediately transferred into a chilled (2–5 °C) nitrogen purged UV oven and cured with UV light (λ=365 nm, power =20 mW/cm^2) for 3 min. After curing, the filled mold was placed face down on a thin film of 0.1% 2,000 g/mol poly(vinyl alcohol) (PVOH, Acros) in water on top of another PET sheet. This assembly was placed in a cooler filled with dry ice, allowing the water to freeze and adhere to the particles. After freezing, the mold was peeled away from the particles trapped in the ice layer, and the ice was allowed to melt. RBCMs and water were collected, washed, and concentrated via centrifugation at ca. 21,000 x g (Eppendorf 5417R) to remove any sol fraction from solution. Particles were then suspended in 0.1% 2,000 g/mol PVOH in PBS, pH 7.4 for subsequent experiments.

Intravital Microscopy. Intravital microscopy experiments were performed using an IV-100 laser scanning microscope (Olympus) on female mice of 19- to 24-g body weight. BALB/c (Charles River), C57BL/6, DBA/2, and B10D2 (Jackson Labs) were maintained in clean animal housing at UNC. Hair was removed from the ear, and a tail vein catheter was applied. The mice were anesthetized with isofluorane and placed onto a heated stage (37°C), with their ear immobilized by two sided taping to an aluminum block. Blood vessels were located by illuminating the ear with a bright white light while imaging in the green fluorescence channel. Blood vessels appear dark on the field. A suspension of 300 nm PRINT particles, 15 mg particles/kg mouse weight via a 4 mg/mL

solution of particles in isotonic 9% sucrose solution, was then injected and visualized using a 633-nm laser. For all imaging blood vessels were selected from the approximate same region of the ear to reduce differences in intensity due to depth of the vessel. For experiments with liposomal clodronate mice were injected with 100 µl of 5 mg/mL clodronate in liposomes both IV and IP 24 hrs prior to experiments. Clodronate was purchased from Encapsula, Nashville TN. For microparticle injections 15 mg/kg of particle in a 2 mg/ml PBS suspension was used. For quantum dot experiments a 4 nmol water soluble carboxilated 665-nm emission suspension of qdots were purchased from Ocean NanoTech (Springdale, Arkansas). 5µl of Qdots were suspended in 100 µl of PBS and then IV injected via tail vein. Granulocyte depletion was performed by injecting 1mg of rat anti mouse Ly6-G (GR-1) monoclonal antibody 1a8 (bioXcell USA) IP 3 days and 1 day prior to experiments.

For image analysis of the blood exposure of the particles, the image files from each scan were exported to ImageJ. For ease of analysis, we followed the example of Merkel et al. (Merkel et al., 2011) and stacked the images in groups of 5. We analyzed the region of interest containing vasculature for fluorescent signal prior to particle injection, and in each scan after injection. The background fluorescence value prior to injection was then subtracted from all following fluorescence values. The data was then exported to GraphPad Prism to generate graphs and perform indicated statistical analysis.

Biodistribution. BALB/c and C57BL6 mice were injected with 300nm cylindrical PRINT particles as described above. At 5min, 30min, 2hr, and 24hrs after injection, four mice of each strain were sacrificed by CO_2 asphyxiation followed by cardiac puncture to collect blood. The lungs, kidneys, heart, liver and spleen were collected and kept in PBS on ice. Solid organs were weighed then placed in 2X weight volume of PBS. The organs were then homogenized and PBS was added to each tube to bring it to a known volume. 50µL of organ homogenate was pipetted into a 96 well plate. For blood 50µL of whole blood was plated followed by centrifuging the remaining blood for 5min at 1500RPM to separate plasma and blood cells. 50µL of plasma and cell fraction was then plated. The plates were read using a fluorescent plate reader (BD, USA), and fluorescence values per gram of tissue were calculated.

Flow cytometry of animal samples. Blood was collected by cardiac puncture and added to EDTA tubes. Spleen and inguinal lymph nodes were dissected and placed in FACS buffer (1xPBS +5%FCS) on ice. All samples were kept on ice or at 4°C for the duration of the experiment. 300µl of blood was taken from each sample; red cells were lysed by addition of 2ml of 0.1X PBS for 10sec followed by 2ml of 2X PBS and 10ml FACS buffer. Spleen and lymph nodes were gently dissociated between frosted slides to free cells and filtered through 70µm cell filters. Red cells in spleen samples were lysed by addition of 1ml ACK lysis buffer (Gibco, Grand Island, NY USA) for 1 min followed by 14ml FACS buffer. Cells were blocked with anti-CD16/32 (Fc-block) from BioLegend

(San Diego, CA USA)) 2µl per sample in 10µl for 10min. Mouse cells were then stained with the following antibodies; anti-CD3-FITC (145-211C), CD19-FITC (ebio1D3), CD19-efluor450 (ebio1D3), anti-TCRβ-APC-Cy7 (H57-591) from ebioscience (San Diego, CA USA), anti-CD11c-PacBlue (N418), anti-F4/80-PE (CI:A3-1), CD11b-PE-Cy7 (M1/70), anti-Gr-1-APC-Cy7 (1A8) from BioLegend (San Diego, CA USA), and anti-CD45-PacOrange (MCD4530) from Invitrogen (Grand Island, NY USA). Cells were stained using antibodies at 1: 200 for 30min on ice. Cells were fixed using 2% PFA in PBS. Particle fluorescence in BMM was detected in the far red channel with a 633nm laser. The average fluorescence intensity of live single cells was calculated and reported. All data were collected using LSRII (BD Biosciences, San Jose, CA USA) or CyAn (Beckman Coulter, Brea, CA USA) flow cytometers. Data analysis performed using FlowJo software (Treestar, Ashland, OR USA).

Cell Culture Reagents. BMM's were generated by extracting bone marrow as described previously (Bennett, 1966) from four female BALB/c or C57BL/6 mice and differentiated into macrophages using L-media as previously reported (Englen et al., 1995). After 1 week of differentiation, cells were placed in serum free DMEM media (Sigma). Cells were then washed once with PBS, placed in ice cold PBS + 5% FBS + .5 mM EDTA, and left on ice for 10 min. Cells were then lifted by gentle scraping and pelleted by centrifugation. 350,000 macrophages were then plated on glass coverslips in DMEM supplemented with 10% FBS (HyClone USA), L-Glutamine, and penicillin/streptomycin for microscopy, or plated under the same media conditions in a 24 well plate for

flow cytometry experiments. For cytokine stimulation, we followed a previously published protocol for in vitro differentiation of macrophages (Martinez et al., 2006). Briefly, cells were exposed to 1 µg/ml LPS (InvivoGen USA) and 25 ng/ml interferon gamma (eBioscience USA) for 24 hrs for M1 stimulation. Cells were cultured with 25 ng/ml IL-4 (eBioscience USA) for M2 stimulation. Human macrophages were generated using a previously published protocol (Beyer et al., 2012). Briefly, peripheral blood monocytes were collected from two healthy male volunteers, cells were then plated on 15cm dishes in DMEM supplemented with 10% FBS, L-Glutamine, penicillin/streptomycin, and 100ng/ml human M-CSF (eBiosciences USA) for seven days. After culture, cells were lifted from 15cm plates as described for BMM's and plated in 24 well plates for 48hrs. Macrophages were then left untreated (control) or supplemented with 1 µg/ml LPS and 25ng/ml human interferon gamma (eBiosciences USA), or human IL-4 25ng/ml (eBiosciences USA) for 24hrs to generate M1 or M2 macropahges respectively. For MMR blocking 5 mg/ml mannan from *Saccharomyces cerevisiae* (Invitrogen) was added to cells for 5 min prior to the addition of particles.

Particle Uptake. For confocal microscopy particle uptake experiments, stock media was made with 75 µg/ml of 300 nm PRINT particles. Media on the cells was then exchanged for media + FBS + particles. Cells were returned to the incubator for 20 min. Media with particles was removed and cells were washed 3X with warm PBS + 5% FBS to remove particles, then 2X with PBS-serum.

Cells were then fixed with ice cold 4% paraformaldehyde in Krebs buffer. Cells were permeabilized with 0.1% Triton in PBS for 5 min. F-actin was stained with Alexa 488 phalloidin (Invitrogen). Coverslips were mounted on glass slides. For flow cytometry, cells were exposed to particles and washed as described for microscopy. After washing cells were placed in ice cold PBS supplemented with 5% FBS and 0.5mM ETDA on ice for 10min followed by gentle scraping to remove from plastic.

Fixed Cell Imaging and analysis. Cells were imaged using an Olympus FV1000 laser scanning confocal microscope. Using a 10X objective, Z stacks were taken in 3 random fields of the coverslip in the Alexa 488 channel to image the cell body and Alexa 633 to image the particles. Each Z stack was then exported to ImageJ and turned into 2 maximum intensity projections of the cell body (phalloidin) and the particles. Single cells were then outlined by automated thresholding in the phalloidin channel and particle fluorescence intensity was acquired in the 633 nm channel. A total of 50 random cells were analyzed per coverslip. The results from cells from four mice were then averaged to determine the relative particle uptake.

Flow cytometry of cultured macrophages. Cells were analyzed using a Dako cyan ADP flow cytometer (Beckman Coulter). Live single cells were selected using forward scatter and side scatter. Particle fluorescence was detected in the far red channel with a 633nm laser. The average fluorescence intensity of live

single cells was calculated and reported. All analysis was performed using FlowJo software.

Statistics. All statistical analysis was performed using GraphPad Prism 5. P values less than .05 were considered significant. For t test unpaired two tailed t test was used, for ANOVA tests 1 way ANOVA with Dunnett's post-test was used. All error bars represent ± SEM.

Study approval. Studies with human samples were performed under IRB #12-1858 with approval from the Office of Human Research Ethics at the University of North Carolina Chapel Hill. All animal experiments were performed with approval of the University of North Carolina Institutional Animal Care and Use Committee.

BIBLIOGRAPHY

Abolins, S.R., Pocock, M.J., Hafalla, J.C., Riley, E.M., and Viney, M.E. (2011). Measures of immune function of wild mice, Mus musculus. Mol Ecol *20*, 881-892.

Alexis, F., Pridgen, E., Molnar, L.K., and Farokhzad, O.C. (2008). Factors affecting the clearance and biodistribution of polymeric nanoparticles. Mol Pharm *5*, 505-515.

Arnold, L., Tyagi, R.K., Mejia, P., Van Rooijen, N., Perignon, J.L., and Druilhe, P. (2010). Analysis of innate defences against Plasmodium falciparum in immunodeficient mice. Malar J *9*, 197.

Auffray, C., Fogg, D., Garfa, M., Elain, G., Join-Lambert, O., Kayal, S., Sarnacki, S., Cumano, A., Lauvau, G., and Geissmann, F. (2007). Monitoring of blood vessels and tissues by a population of monocytes with patrolling behavior. Science *317*, 666-670.

Bakalova, R. (2007). Fluorescent molecular sensors and multi-photon microscopy in brain studies. Brain Res Bull *73*, 150-153.

Bala, S., Tang, A., Catalano, D., Petrasek, J., Taha, O., Kodys, K., and Szabo, G. (2012). Induction of Bcl-3 by acute binge alcohol results in toll-like receptor 4/LPS tolerance. J Leukoc Biol *92*, 611-620.

Bartneck, M., Keul, H.A., Zwadlo-Klarwasser, G., and Groll, J. (2010). Phagocytosis independent extracellular nanoparticle clearance by human immune cells. Nano Lett *10*, 59-63.

Beech, J.R., Shin, S.J., Smith, J.A., and Kelly, K.A. (2013). Mechanisms for Targeted Delivery of Nanoparticles in Cancer. Curr Pharm Des.

Bennett, B. (1966). Isolation and cultivation in vitro of macrophages from various sources in the mouse. Am J Pathol *48*, 165-181.

Benninger, R.K., Hao, M., and Piston, D.W. (2008). Multi-photon excitation imaging of dynamic processes in living cells and tissues. Rev Physiol Biochem Pharmacol *160*, 71-92.

Beyer, M., Mallmann, M.R., Xue, J., Staratschek-Jox, A., Vorholt, D., Krebs, W., Sommer, D., Sander, J., Mertens, C., Nino-Castro, A.*, et al.* (2012). High-resolution transcriptome of human macrophages. PLoS One *7*, e45466.

Biganzoli, L., Coleman, R., Minisini, A., Hamilton, A., Aapro, M., Therasse, P., Mottino, G., Bogaerts, J., and Piccart, M. (2007). A joined analysis of two European Organization for the Research and Treatment of Cancer (EORTC) studies to evaluate the role of pegylated liposomal doxorubicin (Caelyx) in the treatment of elderly patients with metastatic breast cancer. Crit Rev Oncol Hematol *61*, 84-89.

Bishton, M., and Chopra, R. (2004). The role of granulocyte transfusions in neutropenic patients. Br J Haematol *127*, 501-508.

Biswas, S.K., Chittezhath, M., Shalova, I.N., and Lim, J.Y. (2012). Macrophage polarization and plasticity in health and disease. Immunol Res *53*, 11-24.

Blum, J.S., Wearsch, P.A., and Cresswell, P. (2013). Pathways of antigen processing. Annu Rev Immunol *31*, 443-473.

Bortolami, M., Venturi, C., Giacomelli, L., Scalerta, R., Bacchetti, S., Marino, F., Floreani, A., Lise, M., Naccarato, R., and Farinati, F. (2002). Cytokine, infiltrating macrophage and T cell-mediated response to development of primary and secondary human liver cancer. Dig Liver Dis *34*, 794-801.

Boswell, M.G., Zhou, W., Newcomb, D.C., and Peebles, R.S., Jr. (2011). PGI2 as a regulator of CD4+ subset differentiation and function. Prostaglandins Other Lipid Mediat *96*, 21-26.

Brembilla, N.C., and Chizzolini, C. (2012). T cell abnormalities in systemic sclerosis with a focus on Th17 cells. Eur Cytokine Netw *23*, 128-139.

Camilleri, J.P., Williams, A.S., Amos, N., Douglas-Jones, A.G., Love, W.G., and Williams, B.D. (1995). The effect of free and liposome-encapsulated clodronate on the hepatic mononuclear phagocyte system in the rat. Clin Exp Immunol *99*, 269-275.

Canaria, C.A., and Lansford, R. (2010). Advanced optical imaging in living embryos. Cell Mol Life Sci *67*, 3489-3497.

Caron, W.P., Song, G., Kumar, P., Rawal, S., and Zamboni, W.C. (2012). Interpatient pharmacokinetic and pharmacodynamic variability of carrier-mediated anticancer agents. Clin Pharmacol Ther *91*, 802-812.

Chakraborty, C., Pal, S., C, G.D., Wen, Z.H., and Lin, C.S. (2013). Nanoparticles as smart pharmaceutical delivery. Front Biosci *18*, 1030-1050.

Chattopadhyay, S. (2013). Aerosol generation using nanometer liposome suspensions for pulmonary drug delivery applications. J Liposome Res.
Cheng, S.H., Li, F.C., Souris, J.S., Yang, C.S., Tseng, F.G., Lee, H.S., Chen, C.T., Dong, C.Y., and Lo, L.W. (2012). Visualizing dynamics of sub-hepatic

distribution of nanoparticles using intravital multiphoton fluorescence microscopy. ACS Nano *6*, 4122-4131.

Chinetti-Gbaguidi, G., Baron, M., Bouhlel, M.A., Vanhoutte, J., Copin, C., Sebti, Y., Derudas, B., Mayi, T., Bories, G., Tailleux, A.*, et al.* (2011). Human atherosclerotic plaque alternative macrophages display low cholesterol handling but high phagocytosis because of distinct activities of the PPARgamma and LXRalpha pathways. Circ Res *108*, 985-995.

Chu, K.S., Hasan, W., Rawal, S., Walsh, M.D., Enlow, E.M., Luft, J.C., Bridges, A.S., Kuijer, J.L., Napier, M.E., Zamboni, W.C.*, et al.* (2012). Plasma, tumor and tissue pharmacokinetics of Docetaxel delivered via nanoparticles of different sizes and shapes in mice bearing SKOV-3 human ovarian carcinoma xenograft. Nanomedicine.

Churchill, G.A., Airey, D.C., Allayee, H., Angel, J.M., Attie, A.D., Beatty, J., Beavis, W.D., Belknap, J.K., Bennett, B., Berrettini, W.*, et al.* (2004). The Collaborative Cross, a community resource for the genetic analysis of complex traits. Nature genetics *36*, 1133-1137.

Coleman, R.E., Biganzoli, L., Canney, P., Dirix, L., Mauriac, L., Chollet, P., Batter, V., Ngalula-Kabanga, E., Dittrich, C., and Piccart, M. (2006). A randomised phase II study of two different schedules of pegylated liposomal doxorubicin in metastatic breast cancer (EORTC-10993). Eur J Cancer *42*, 882-887.

Cope, A., Le Friec, G., Cardone, J., and Kemper, C. (2011). The Th1 life cycle: molecular control of IFN-gamma to IL-10 switching. Trends Immunol *32*, 278-286.

Crispe, I.N. (2009). The liver as a lymphoid organ. Annu Rev Immunol *27*, 147-163.

Cudejko, C., Wouters, K., Fuentes, L., Hannou, S.A., Paquet, C., Bantubungi, K., Bouchaert, E., Vanhoutte, J., Fleury, S., Remy, P*., et al.* (2011). p16INK4a deficiency promotes IL-4-induced polarization and inhibits proinflammatory signaling in macrophages. Blood *118*, 2556-2566.
den Haan, J.M., and Kraal, G. (2012). Innate immune functions of macrophage subpopulations in the spleen. J Innate Immun *4*, 437-445.

Dreaden, E.C., Alkilany, A.M., Huang, X., Murphy, C.J., and El-Sayed, M.A. (2012a). The golden age: gold nanoparticles for biomedicine. Chem Soc Rev *41*, 2740-2779.
Dreaden, E.C., Austin, L.A., Mackey, M.A., and El-Sayed, M.A. (2012b). Size matters: gold nanoparticles in targeted cancer drug delivery. Ther Deliv *3*, 457-478.

Durafourt, B.A., Moore, C.S., Zammit, D.A., Johnson, T.A., Zaguia, F., Guiot, M.C., Bar-Or, A., and Antel, J.P. (2012). Comparison of polarization properties of human adult microglia and blood-derived macrophages. Glia *60*, 717-727.

Englen, M.D., Valdez, Y.E., Lehnert, N.M., and Lehnert, B.E. (1995). Granulocyte/macrophage colony-stimulating factor is expressed and secreted in cultures of murine L929 cells. J Immunol Methods *184*, 281-283.

Fehres, C.M., Garcia-Vallejo, J.J., Unger, W.W., and van Kooyk, Y. (2013). Skin-resident antigen-presenting cells: instruction manual for vaccine development. Front Immunol *4*, 157.

Fels, A.O., and Cohn, Z.A. (1986). The alveolar macrophage. Journal of applied physiology *60*, 353-369.

Feng, L., Zhu, C., Yuan, H., Liu, L., Lv, F., and Wang, S. (2013). Conjugated polymer nanoparticles: preparation, properties, functionalization and biological applications. Chem Soc Rev.

Fernandez-Urrusuno, R., Fattal, E., Rodrigues, J.M., Jr., Feger, J., Bedossa, P., and Couvreur, P. (1996). Effect of polymeric nanoparticle administration on the clearance activity of the mononuclear phagocyte system in mice. J Biomed Mater Res *31*, 401-408.

Fitrolaki, D.M., Dimitriou, H., Kalmanti, M., and Briassoulis, G. (2013). CD64-Neutrophil expression and stress metabolic patterns in early sepsis and severe traumatic brain injury in children. BMC Pediatr *13*, 31.

Fokong, S., Theek, B., Wu, Z., Koczera, P., Appold, L., Jorge, S., Resch-Genger, U., van Zandvoort, M., Storm, G., Kiessling, F*., et al.* (2012). Image-guided, targeted and triggered drug delivery to tumors using polymer-based microbubbles. J Control Release *163*, 75-81.

Frasinariu, O.E., Ceccarelli, S., Alisi, A., Moraru, E., and Nobili, V. (2013). Gut-liver axis and fibrosis in nonalcoholic fatty liver disease: An input for novel therapies. Dig Liver Dis *45*, 543-551.

Frevert, U., Usynin, I., Baer, K., and Klotz, C. (2008). Plasmodium sporozoite passage across the sinusoidal cell layer. Subcell Biochem *47*, 182-197.

Ganz, T. (2012). Macrophages and systemic iron homeostasis. J Innate Immun *4*, 446-453.

Garaschuk, O., Milos, R.I., Grienberger, C., Marandi, N., Adelsberger, H., and Konnerth, A. (2006). Optical monitoring of brain function in vivo: from neurons to networks. Pflugers Arch *453*, 385-396.

Garay, R.P., El-Gewely, R., Armstrong, J.K., Garratty, G., and Richette, P. (2012). Antibodies against polyethylene glycol in healthy subjects and in patients treated with PEG-conjugated agents. Expert Opin Drug Deliv.

Geissmann, F., Manz, M.G., Jung, S., Sieweke, M.H., Merad, M., and Ley, K. (2010). Development of monocytes, macrophages, and dendritic cells. Science *327*, 656-661.

Gordon, S., and Martinez, F.O. (2010). Alternative activation of macrophages: mechanism and functions. Immunity *32*, 593-604.

Gradishar, W. (2006a). Landmark trials in endocrine adjuvant therapy for breast carcinoma. Cancer *106*, 975-981.

Gradishar, W.J. (2006b). Albumin-bound paclitaxel: a next-generation taxane. Expert Opin Pharmacother *7*, 1041-1053.

Gratton, S.E., Napier, M.E., Ropp, P.A., Tian, S., and DeSimone, J.M. (2008a). Microfabricated particles for engineered drug therapies: elucidation into the mechanisms of cellular internalization of PRINT particles. Pharmaceutical research *25*, 2845-2852.

Gratton, S.E., Pohlhaus, P.D., Lee, J., Guo, J., Cho, M.J., and Desimone, J.M. (2007). Nanofabricated particles for engineered drug therapies: a preliminary biodistribution study of PRINT nanoparticles. Journal of controlled release : official journal of the Controlled Release Society *121*, 10-18.

Gratton, S.E., Ropp, P.A., Pohlhaus, P.D., Luft, J.C., Madden, V.J., Napier, M.E., and DeSimone, J.M. (2008b). The effect of particle design on cellular internalization pathways. Proc Natl Acad Sci U S A *105*, 11613-11618.

Gratton, S.E., Williams, S.S., Napier, M.E., Pohlhaus, P.D., Zhou, Z., Wiles, K.B., Maynor, B.W., Shen, C., Olafsen, T., Samulski, E.T.*, et al.* (2008c). The pursuit of a scalable nanofabrication platform for use in material and life science applications. Accounts of chemical research *41*, 1685-1695.

Gregory, S.H., Cousens, L.P., van Rooijen, N., Dopp, E.A., Carlos, T.M., and Wing, E.J. (2002). Complementary adhesion molecules promote neutrophil-Kupffer cell interaction and the elimination of bacteria taken up by the liver. J Immunol *168*, 308-315.

Gregory, S.H., and Wing, E.J. (2002). Neutrophil-Kupffer cell interaction: a critical component of host defenses to systemic bacterial infections. J Leukoc Biol *72*, 239-248.

Grogan, J.L., and Locksley, R.M. (2002). T helper cell differentiation: on again, off again. Current opinion in immunology *14*, 366-372.

Gu, Z., Yan, L., Tian, G., Li, S., Chai, Z., and Zhao, Y. (2013). Recent Advances in Design and Fabrication of Upconversion Nanoparticles and Their Safe

Theranostic Applications. Adv Mater.

Guery, L., and Hugues, S. (2013). Tolerogenic and activatory plasmacytoid dendritic cells in autoimmunity. Front Immunol *4*, 59.

Hak, S., Reitan, N.K., Haraldseth, O., and de Lange Davies, C. (2010). Intravital microscopy in window chambers: a unique tool to study tumor angiogenesis and delivery of nanoparticles. Angiogenesis *13*, 113-130.

Illum, L., and Davis, S.S. (1984). The organ uptake of intravenously administered colloidal particles can be altered using a non-ionic surfactant (Poloxamer 338). FEBS Lett *167*, 79-82.

Illum, L., Jones, P.D., Baldwin, R.W., and Davis, S.S. (1984). Tissue distribution of poly(hexyl 2-cyanoacrylate) nanoparticles coated with monoclonal antibodies in mice bearing human tumor xenografts. J Pharmacol Exp Ther *230*, 733-736.

Ishihara, T., Takeda, M., Sakamoto, H., Kimoto, A., Kobayashi, C., Takasaki, N., Yuki, K., Tanaka, K., Takenaga, M., Igarashi, R.*, et al.* (2009). Accelerated blood clearance phenomenon upon repeated injection of PEG-modified PLA-nanoparticles. Pharm Res *26*, 2270-2279.

Jolck, R.I., Berg, R.H., and Andresen, T.L. (2010). Solid-phase synthesis of PEGylated lipopeptides using click chemistry. Bioconjug Chem *21*, 807-810.

Kastrukoff, L.F., Lau, A.S., and Thomas, E.E. (2012). The effect of mouse strain on herpes simplex virus type 1 (HSV-1) infection of the central nervous system (CNS). Herpesviridae *3*, 4.

Knoferl, M.W., Angele, M.K., Diodato, M.D., Schwacha, M.G., Ayala, A., Cioffi, W.G., Bland, K.I., and Chaudry, I.H. (2002). Female sex hormones regulate macrophage function after trauma-hemorrhage and prevent increased death rate from subsequent sepsis. Ann Surg *235*, 105-112.

Koek, G.H., Liedorp, P.R., and Bast, A. (2011). The role of oxidative stress in non-alcoholic steatohepatitis. Clin Chim Acta *412*, 1297-1305.

Kono, H., Fujii, H., Ogiku, M., Hara, M., Tsuchiya, M., Ishii, K., and Hosomura, N. (2012). The Kupffer cell inhibition exacerbates but splenectomy prevents mortality in a rat septic peritonitis model. J Surg Res *175*, 101-112.

Kovtunovych, G., Eckhaus, M.A., Ghosh, M.C., Ollivierre-Wilson, H., and Rouault, T.A. (2010). Dysfunction of the heme recycling system in heme oxygenase 1-deficient mice: effects on macrophage viability and tissue iron distribution. Blood *116*, 6054-6062.

Krown, S.E., Northfelt, D.W., Osoba, D., and Stewart, J.S. (2004). Use of liposomal anthracyclines in Kaposi's sarcoma. Semin Oncol *31*, 36-52.

Krysko, O., Holtappels, G., Zhang, N., Kubica, M., Deswarte, K., Derycke, L., Claeys, S., Hammad, H., Brusselle, G.G., Vandenabeele, P.*, et al.* (2011). Alternatively activated macrophages and impaired phagocytosis of S. aureus in chronic rhinosinusitis. Allergy *66*, 396-403.

Kulkarni, S.A., and Feng, S.S. (2013). Effects of Particle Size and Surface Modification on Cellular Uptake and Biodistribution of Polymeric Nanoparticles for Drug Delivery. Pharm Res.

Lammers, T., Kiessling, F., Hennink, W.E., and Storm, G. (2012). Drug targeting to tumors: principles, pitfalls and (pre-) clinical progress. J Control Release *161*, 175-187.

Lentz, T.B., Gray, S.J., and Samulski, R.J. (2012). Viral vectors for gene delivery to the central nervous system. Neurobiol Dis *48*, 179-188.

Leuschner, F., Dutta, P., Gorbatov, R., Novobrantseva, T.I., Donahoe, J.S., Courties, G., Lee, K.M., Kim, J.I., Markmann, J.F., Marinelli, B.*, et al.* (2011). Therapeutic siRNA silencing in inflammatory monocytes in mice. Nat Biotechnol *29*, 1005-1010.

Li, C., Bolisetty, S., Chaitanya, K., Adamcik, J., and Mezzenga, R. (2013a). Tunable carbon nanotube/protein core-shell nanoparticles with NIR- and enzymatic-responsive cytotoxicity. Adv Mater *25*, 1010-1015.

Li, X., Zhao, Q., and Qiu, L. (2013b). Smart ligand: Aptamer-mediated targeted delivery of chemotherapeutic drugs and siRNA for cancer therapy. J Control Release.

Liu, J., Gu, C., Cabigas, E.B., Pendergrass, K.D., Brown, M.E., Luo, Y., and Davis, M.E. (2013). Functionalized dendrimer-based delivery of angiotensin type 1 receptor siRNA for preserving cardiac function following infarction. Biomaterials *34*, 3729-3736.

Ma, N., Ma, C., Deng, Y., Wang, T., and He, N. (2013). Advances in applications of dendritic compounds. J Nanosci Nanotechnol *13*, 33-39.

Manfredi, A.A., Rovere-Querini, P., and Maugeri, N. (2010). Dangerous connections: neutrophils and the phagocytic clearance of activated platelets. Curr Opin Hematol *17*, 3-8.

Manjila, S.B., Baby, J.N., Bijin, E.N., Constantine, I., Pramod, K., and Valsalakumari, J. (2013). Novel gene delivery systems. Int J Pharm Investig *3*, 1-7.

Mantovani, A., Sozzani, S., Locati, M., Allavena, P., and Sica, A. (2002). Macrophage polarization: tumor-associated macrophages as a paradigm for polarized M2 mononuclear phagocytes. Trends Immunol *23*, 549-555.

Martinez, F.O., Gordon, S., Locati, M., and Mantovani, A. (2006). Transcriptional profiling of the human monocyte-to-macrophage differentiation and polarization: new molecules and patterns of gene expression. J Immunol *177*, 7303-7311.

Maugeri, N., Baldini, M., Ramirez, G.A., Rovere-Querini, P., and Manfredi, A.A. (2012). Platelet-leukocyte deregulated interactions foster sterile inflammation

and tissue damage in immune-mediated vessel diseases. Thromb Res *129*, 267-273.

Maugeri, N., Rovere-Querini, P., Evangelista, V., Covino, C., Capobianco, A., Bertilaccio, M.T., Piccoli, A., Totani, L., Cianflone, D., Maseri, A.*, et al.* (2009). Neutrophils phagocytose activated platelets in vivo: a phosphatidylserine, P-selectin, and {beta}2 integrin-dependent cell clearance program. Blood *113*, 5254-5265.

Merkel, T.J., Jones, S.W., Herlihy, K.P., Kersey, F.R., Shields, A.R., Napier, M., Luft, J.C., Wu, H., Zamboni, W.C., Wang, A.Z.*, et al.* (2011). Using mechanobiological mimicry of red blood cells to extend circulation times of hydrogel microparticles. Proc Natl Acad Sci U S A *108*, 586-591.

Merrill, W. (1990). Lung defence mechanisms against infection. Eur Respir J *3*, 372-373.

Mesquita, R.C., Han, S.W., Miller, J., Schenkel, S.S., Pole, A., Esipova, T.V., Vinogradov, S.A., Putt, M.E., Yodh, A.G., and Busch, T.M. (2012). Tumor Blood Flow Differs between Mouse Strains: Consequences for Vasoresponse to Photodynamic Therapy. PLoS One *7*, e37322.

Mestas, J., and Hughes, C.C. (2004). Of mice and not men: differences between mouse and human immunology. J Immunol *172*, 2731-2738.

Mills, C.D., Kincaid, K., Alt, J.M., Heilman, M.J., and Hill, A.M. (2000). M-1/M-2 macrophages and the Th1/Th2 paradigm. J Immunol *164*, 6166-6173.

Miyata, R., and van Eeden, S.F. (2011). The innate and adaptive immune response induced by alveolar macrophages exposed to ambient particulate matter. Toxicol Appl Pharmacol *257*, 209-226.

Moghimi, S.M., Parhamifar, L., Ahmadvand, D., Wibroe, P.P., Andresen, T.L., Farhangrazi, Z.S., and Hunter, A.C. (2012). Particulate systems for targeting of macrophages: basic and therapeutic concepts. J Innate Immun *4*, 509-528.

Mogil, J.S., Wilson, S.G., Bon, K., Lee, S.E., Chung, K., Raber, P., Pieper, J.O., Hain, H.S., Belknap, J.K., Hubert, L.*, et al.* (1999). Heritability of nociception I: responses of 11 inbred mouse strains on 12 measures of nociception. Pain *80*, 67-82.

Morachis, J.M., Mahmoud, E.A., and Almutairi, A. (2012a). Physical and chemical strategies for therapeutic delivery by using polymeric nanoparticles. Pharmacol Rev *64*, 505-519.

Morachis, J.M., Mahmoud, E.A., Sankaranarayanan, J., and Almutairi, A. (2012b). Triggered rapid degradation of nanoparticles for gene delivery. J Drug Deliv *2012*, 291219.

Moselhy, J., Wu, X.Y., Nicholov, R., and Kodaria, K. (2000). In vitro studies of the interaction of poly(NIPAm/MAA) nanoparticles with proteins and cells. J Biomater Sci Polym Ed *11*, 123-147.

Muranski, P., and Restifo, N.P. (2013). Essentials of Th17 cell commitment and plasticity. Blood *121*, 2402-2414.

Murphy, K.M., and Reiner, S.L. (2002). The lineage decisions of helper T cells. Nat Rev Immunol *2*, 933-944.

Muthiah, M., Park, I.K., and Cho, C.S. (2013). Nanoparticle-mediated delivery of therapeutic genes: focus on miRNA therapeutics. Expert Opin Drug Deliv.

Naik, S.R., Desai, S.K., Shah, P.D., and Wala, S.M. (2013). Liposomes as Potential Carrier System for Targeted Delivery of Polyene Antibiotics. Recent Pat Inflamm Allergy Drug Discov.

Nakano, Y., Hisaeda, H., Sakai, T., Zhang, M., Maekawa, Y., Zhang, T., and Himeno, K. (2001). Role of innate immune cells in protection against Toxoplasma gondii at inflamed site. J Med Invest *48*, 73-80.

Nel, A.E., Madler, L., Velegol, D., Xia, T., Hoek, E.M.V., Somasundaran, P., Klaessig, F., Castranova, V., and Thompson, M. (2009). Understanding biophysicochemical interactions at the nano-bio interface. Nature Materials *8*, 543-557.

Niesner, R.A., and Hauser, A.E. (2011). Recent advances in dynamic intravital multi-photon microscopy. Cytometry A *79*, 789-798.

Nishio, K., Qiao, S., and Yamashita, H. (2005). Characterization of the differential expression of uncoupling protein 2 and ROS production in differentiated mouse macrophage-cells (Mm1) and the progenitor cells (M1). Journal of molecular histology *36*, 35-44.

Noel, W., Raes, G., Hassanzadeh Ghassabeh, G., De Baetselier, P., and Beschin, A. (2004). Alternatively activated macrophages during parasite infections. Trends Parasitol *20*, 126-133.

Novak, M.L., and Koh, T.J. (2013). Macrophage phenotypes during tissue repair. Journal of leukocyte biology *93*, 875-881.

Ogiku, M., Kono, H., Ishii, K., Hosomura, N., and Fujii, H. (2011). Role of macrophage colony-stimulating factor in polymicrobial sepsis according to studies using osteopetrotic (op/op) mice. J Surg Res *169*, 106-116.

Owens, D.E., 3rd, and Peppas, N.A. (2006). Opsonization, biodistribution, and pharmacokinetics of polymeric nanoparticles. Int J Pharm *307*, 93-102.

Papahadjopoulos, D., Allen, T.M., Gabizon, A., Mayhew, E., Matthay, K., Huang, S.K., Lee, K.D., Woodle, M.C., Lasic, D.D., Redemann, C.*, et al.* (1991). Sterically stabilized liposomes: improvements in pharmacokinetics and antitumor therapeutic efficacy. Proc Natl Acad Sci U S A *88*, 11460-11464.

Pardeshi, C., Rajput, P., Belgamwar, V., Tekade, A., Patil, G., Chaudhary, K., and Sonje, A. (2012). Solid lipid based nanocarriers: An overview / Nanonosaci na bazi cvrstih lipida: Pregled. Acta Pharm *62*, 433-472.

Patel, P.C., Giljohann, D.A., Daniel, W.L., Zheng, D., Prigodich, A.E., and Mirkin, C.A. (2010). Scavenger receptors mediate cellular uptake of polyvalent oligonucleotide-functionalized gold nanoparticles. Bioconjug Chem *21*, 2250-2256.

Paulnock, D.M. (1992). Macrophage activation by T cells. Current opinion in immunology *4*, 344-349.

Pearce, E.J., and Reiner, S.L. (1995). Induction of Th2 responses in infectious diseases. Current opinion in immunology *7*, 497-504.

Perry, J.L., Reuter, K.G., Kai, M.P., Herlihy, K.P., Jones, S.W., Luft, J.C., Napier, M., Bear, J.E., and Desimone, J.M. (2012). PEGylated PRINT Nanoparticles: The Impact of PEG Density on Protein Binding, Macrophage Association, Biodistribution, and Pharmacokinetics. Nano Lett.

Petkova, S.B., Yuan, R., Tsaih, S.W., Schott, W., Roopenian, D.C., and Paigen, B. (2008). Genetic influence on immune phenotype revealed strain-specific variations in peripheral blood lineages. Physiol Genomics *34*, 304-314.

Petrasek, J., Bala, S., Csak, T., Lippai, D., Kodys, K., Menashy, V., Barrieau, M., Min, S.Y., Kurt-Jones, E.A., and Szabo, G. (2012). IL-1 receptor antagonist ameliorates inflammasome-dependent alcoholic steatohepatitis in mice. J Clin Invest *122*, 3476-3489.

Pittman, K., and Kubes, P. (2013). Damage-associated molecular patterns control neutrophil recruitment. J Innate Immun *5*, 315-323.
Pulendran, B., and Artis, D. (2012). New paradigms in type 2 immunity. Science *337*, 431-435.

Purohit, V., and Brenner, D.A. (2006). Mechanisms of alcohol-induced hepatic fibrosis: a summary of the Ron Thurman Symposium. Hepatology *43*, 872-878.
Qian, S., Li, C., and Zuo, Z. (2012). Pharmacokinetics and disposition of various drug loaded liposomes. Curr Drug Metab *13*, 372-395.

Rabinovitch, M. (1995). Professional and non-professional phagocytes: an introduction. Trends Cell Biol *5*, 85-87.

Randolph, G.J., Jakubzick, C., and Qu, C. (2008). Antigen presentation by monocytes and monocyte-derived cells. Curr Opin Immunol *20*, 52-60.

Ravina, M., Paolicelli, P., Seijo, B., and Sanchez, A. (2010). Knocking down gene expression with dendritic vectors. Mini Rev Med Chem *10*, 73-86.

Reynolds, N.P., Styan, K.E., Easton, C.D., Li, Y., Waddington, L., Lara, C., Forsythe, J.S., Mezzenga, R., Hartley, P.G., and Muir, B.W. (2013). Nanotopographic surfaces with defined surface chemistries from amyloid fibril networks can control cell attachment. Biomacromolecules *14*, 2305-2316.

Rolland, J.P., Maynor, B.W., Euliss, L.E., Exner, A.E., Denison, G.M., and DeSimone, J.M. (2005). Direct fabrication and harvesting of monodisperse, shape-specific nanobiomaterials. J Am Chem Soc *127*, 10096-10100.

Romagnani, S. (2008). Human Th17 cells. Arthritis Res Ther *10*, 206.
Sahay, G., Alakhova, D.Y., and Kabanov, A.V. (2010). Endocytosis of nanomedicines. J Control Release *145*, 182-195.

Sawada, K., Ohtake, T., Hasebe, T., Abe, M., Tanaka, H., Ikuta, K., Suzuki, Y., Fujiya, M., Hasebe, C., and Kohgo, Y. (2013). Augmented hepatic Toll-like receptors by fatty acids trigger the pro-inflammatory state of nonalcoholic fatty liver disease in mice. Hepatol Res.
Schmitt, E.G., and Williams, C.B. (2013). Generation and function of induced regulatory T cells. Front Immunol *4*, 152.

Shih-Ching, K., Choudhry, M.A., Matsutani, T., Schwacha, M.G., Rue, L.W., Bland, K.I., and Chaudry, I.H. (2004). Splenectomy differentially influences immune responses in various tissue compartments of the body. Cytokine *28*, 101-108.

Shimizu, T., Ichihara, M., Yoshioka, Y., Ishida, T., Nakagawa, S., and Kiwada, H. (2012). Intravenous Administration of Polyethylene Glycol-Coated (PEGylated) Proteins and PEGylated Adenovirus Elicits an Anti-PEG Immunoglobulin M Response. Biol Pharm Bull *35*, 1336-1342.

Shin, S.J., Beech, J.R., and Kelly, K.A. (2013). Targeted nanoparticles in imaging: paving the way for personalized medicine in the battle against cancer. Integr Biol (Camb) *5*, 29-42.

Shou, J., Motyka, L.E., and Daly, J.M. (1994). Intestinal microbial translocation: immunologic consequences and effects of interleukin-4. Surgery *116*, 868-876.

Silva, M.T., and Correia-Neves, M. (2012). Neutrophils and macrophages: the main partners of phagocyte cell systems. Front Immunol *3*, 174.

Singha, K., Namgung, R., and Kim, W.J. (2011). Polymers in small-interfering RNA delivery. Nucleic Acid Ther *21*, 133-147.

Smith, B.R., Cheng, Z., De, A., Koh, A.L., Sinclair, R., and Gambhir, S.S. (2008). Real-time intravital imaging of RGD-quantum dot binding to luminal endothelium in mouse tumor neovasculature. Nano Lett *8*, 2599-2606.

Smith, B.R., Cheng, Z., De, A., Rosenberg, J., and Gambhir, S.S. (2010). Dynamic visualization of RGD-quantum dot binding to tumor neovasculature and extravasation in multiple living mouse models using intravital microscopy. Small *6*, 2222-2229.

Smith, B.R., Kempen, P., Bouley, D., Xu, A., Liu, Z., Melosh, N., Dai, H., Sinclair, R., and Gambhir, S.S. (2012). Shape matters: intravital microscopy reveals surprising geometrical dependence for nanoparticles in tumor models of extravasation. Nano Lett *12*, 3369-3377.

Stadecker, M.J., Asahi, H., Finger, E., Hernandez, H.J., Rutitzky, L.I., and Sun, J. (2004). The immunobiology of Th1 polarization in high-pathology schistosomiasis. Immunol Rev *201*, 168-179.

Sumen, C., Mempel, T.R., Mazo, I.B., and von Andrian, U.H. (2004). Intravital microscopy: visualizing immunity in context. Immunity *21*, 315-329.

Sun, X., Sun, H., Li, H., and Peng, H. (2013a). Developing Polymer Composite Materials: Carbon Nanotubes or Graphene? Adv Mater.

Sun, Y., Zhu, Y., Wang, L., Mao, X., Peng, X., and Peng, Y. (2013b). Recombinant adenovirus-mediated intestinal trefoil factor gene therapy for burn-induced intestinal mucosal injury. PLoS One *8*, e62429.

Swirski, F.K., Nahrendorf, M., Etzrodt, M., Wildgruber, M., Cortez-Retamozo, V., Panizzi, P., Figueiredo, J.L., Kohler, R.H., Chudnovskiy, A., Waterman, P.*, et al.* (2009). Identification of splenic reservoir monocytes and their deployment to inflammatory sites. Science *325*, 612-616.

Szabo, G., Petrasek, J., and Bala, S. (2012). Innate immunity and alcoholic liver disease. Dig Dis *30 Suppl 1*, 55-60.

Tacke, F., Alvarez, D., Kaplan, T.J., Jakubzick, C., Spanbroek, R., Llodra, J., Garin, A., Liu, J., Mack, M., van Rooijen, N.*, et al.* (2007). Monocyte subsets differentially employ CCR2, CCR5, and CX3CR1 to accumulate within atherosclerotic plaques. J Clin Invest *117*, 185-194.

Tan, A., Yildirimer, L., Rajadas, J., De La Pena, H., Pastorin, G., and Seifalian, A. (2011). Quantum dots and carbon nanotubes in oncology: a review on emerging theranostic applications in nanomedicine. Nanomedicine (Lond) *6*, 1101-1114.

Tavares, J., Formaglio, P., Medvinsky, A., Menard, R., and Amino, R. (2013a). Imaging sporozoite cell traversal in the liver of mice. Methods Mol Biol *923*, 401-410.

Tavares, J., Formaglio, P., Thiberge, S., Mordelet, E., Van Rooijen, N., Medvinsky, A., Menard, R., and Amino, R. (2013b). Role of host cell traversal by the malaria sporozoite during liver infection. J Exp Med *210*, 905-915.

Tomita, K., Teratani, T., Suzuki, T., Shimizu, M., Sato, H., Narimatsu, K., Okada, Y., Kurihara, C., Irie, R., Yokoyama, H.*, et al.* (2013). Free cholesterol accumulation in hepatic stellate cells: Mechanism of liver fibrosis aggravation in nonalcoholic steatohepatitis in mice. Hepatology.

Tong, L., He, W., Zhang, Y., Zheng, W., and Cheng, J.X. (2009a). Visualizing systemic clearance and cellular level biodistribution of gold nanorods by intrinsic two-photon luminescence. Langmuir *25*, 12454-12459.

Tong, L., Wei, Q., Wei, A., and Cheng, J.X. (2009b). Gold nanorods as contrast agents for biological imaging: optical properties, surface conjugation and photothermal effects. Photochem Photobiol *85*, 21-32.

Traeger, T., Mikulcak, M., Eipel, C., Abshagen, K., Diedrich, S., Heidecke, C.D., Maier, S., and Vollmar, B. (2010). Kupffer cell depletion reduces hepatic inflammation and apoptosis but decreases survival in abdominal sepsis. Eur J Gastroenterol Hepatol *22*, 1039-1049.

Tugal, D., Liao, X., and Jain, M.K. (2013). Transcriptional control of macrophage polarization. Arteriosclerosis, thrombosis, and vascular biology *33*, 1135-1144.

Tundup, S., Srivastava, L., and Harn, D.A., Jr. (2012). Polarization of host immune responses by helminth-expressed glycans. Annals of the New York Academy of Sciences *1253*, E1-E13.

Uchugonova, A., Zhao, M., Weinigel, M., Zhang, Y., Bouvet, M., Hoffman, R.M., and Konig, K. (2013). Multiphoton tomography visualizes collagen fibers in the tumor microenvironment that maintain cancer-cell anchorage and shape. J Cell Biochem *114*, 99-102.

Usme-Ciro, J.A., Campillo-Pedroza, N., Almazan, F., and Gallego-Gomez, J.C. (2013). Cytoplasmic RNA viruses as potential vehicles for the delivery of therapeutic small RNAs. Virol J *10*, 185.

Van den Eynden, G.G., Majeed, A.W., Illemann, M., Vermeulen, P.B., Bird, N.C., Hoyer-Hansen, G., Eefsen, R.L., Reynolds, A.R., and Brodt, P. (2013). The multifaceted role of the microenvironment in liver metastasis: biology and clinical implications. Cancer Res *73*, 2031-2043.

Vasquez, K.O., Casavant, C., and Peterson, J.D. (2011). Quantitative whole body biodistribution of fluorescent-labeled agents by non-invasive tomographic imaging. PLoS One *6*, e20594.

Wadajkar, A.S., Menon, J.U., Kadapure, T., Tran, R.T., Yang, J., and Nguyen, K.T. (2013). Design and Application of Magnetic-based Theranostic Nanoparticle Systems. Recent Pat Biomed Eng *6*, 47-57.

Wan, J., Benkdane, M., Teixeira-Clerc, F., Bonnafous, S., Louvet, A., Lafdil, F., Pecker, F., Tran, A., Gual, P., Mallat, A.*, et al.* (2013). M2 Kupffer cells promote M1 Kupffer cell apoptosis: A protective mechanism against alcoholic and non-alcoholic fatty liver disease. Hepatology.

Wang, J., Tian, S., Petros, R.A., Napier, M.E., and Desimone, J.M. (2010). The complex role of multivalency in nanoparticles targeting the transferrin receptor for cancer therapies. Journal of the American Chemical Society *132*, 11306-11313.

Wong, R., Shou, J., and Wang, Y. (2010). Probing sepsis and sepsis-like conditions using untargeted SPIO nanoparticles. Conf Proc IEEE Eng Med Biol Soc *2010*, 3053-3056.

Wynn, T.A., Chawla, A., and Pollard, J.W. (2013). Macrophage biology in development, homeostasis and disease. Nature *496*, 445-455.

Wynn, T.A., Freund, Y.R., and Paulnock, D.M. (1992). TNF-alpha differentially regulates Ia antigen expression and macrophage tumoricidal activity in two murine macrophage cell lines. Cellular immunology *140*, 184-196.

Yang, A., Liu, W., Li, Z., Jiang, L., Xu, H., and Yang, X. (2010). Influence of polyethyleneglycol modification on phagocytic uptake of polymeric nanoparticles mediated by immunoglobulin G and complement activation. J Nanosci Nanotechnol *10*, 622-628.

Yildirimer, L., Thanh, N.T., Loizidou, M., and Seifalian, A.M. (2011). Toxicology and clinical potential of nanoparticles. Nano Today *6*, 585-607.

Yoo, J.W., Chambers, E., and Mitragotri, S. (2010). Factors that control the circulation time of nanoparticles in blood: challenges, solutions and future prospects. Curr Pharm Des *16*, 2298-2307.

Yurgel, V., Collares, T., and Seixas, F. (2013). Developments in the use of nanocapsules in oncology. Braz J Med Biol Res *0*.

Zamboni, W.C., Strychor, S., Maruca, L., Ramalingam, S., Zamboni, B.A., Wu, H., Friedland, D.M., Edwards, R.P., Stoller, R.G., Belani, C.P.*, et al.* (2009). Pharmacokinetic study of pegylated liposomal CKD-602 (S-CKD602) in patients with advanced malignancies. Clin Pharmacol Ther *86*, 519-526.

Zamboni, W.C., Torchilin, V., Patri, A.K., Hrkach, J., Stern, S., Lee, R., Nel, A., Panaro, N.J., and Grodzinski, P. (2012). Best Practices in Cancer Nanotechnology: Perspective from NCI Nanotechnology Alliance. Clin Cancer Res *18*, 3229-3241.

Zhang, G., Zeng, X., and Li, P. (2013). Nanomaterials in cancer-therapy drug delivery system. J Biomed Nanotechnol *9*, 741-750.